Impact of functional studies on exome sequence variant interpretation in early-onset cardiac conduction system diseases

Kenshi Hayashi, Ryota Teramoto, Akihiro Nomura, Yoshihiro Asano, Manu Beerens, Yasutaka Kurata, Isao Kobayashi, Noboru Fujino, Hiroshi Furusho, Kenji Sakata, Kenji Onoue, David Y Chiang, Tuomas O Kiviniemi, Eva Buys, Patrick Sips, Micah L Burch, Yanbin Zhao, Amy E Kelly, Masanobu Namura, Yoshihito Kita, Taketsugu Tsuchiya, Bunji Kaku, Kotaro Oe, Yuko Takeda, Tetsuo Konno, Masaru Inoue, Takashi Fujita, Takeshi Kato, Akira Funada, Hayato Tada, Akihiko Hodatsu, Chiaki Nakanishi, Yuichiro Sakamoto, Toyonobu Tsuda, Yoji Nagata, Yoshihiro Tanaka, Hirofumi Okada, Keiich Usuda, Shihe Cui, Yoshihiko Saito, Calum A MacRae, Seiji Takashima, Masakazu Yamagishi, Masa-aki Kawashiri, Masayuki Takamura

In: Cardiovascular Research, cvaa010, 2020

https://doi.org/10.1093/cvr/cvaa010

Impact of functional studies on exome sequence variant interpretation in early-onset cardiac conduction system diseases

Kenshi Hayashi[1], Akihiro Nomura[1], Ryota Teramoto[1,2], Yoshihiro Asano[3], Manu Beerens[2], Yasutaka Kurata[4], Noboru Fujino[1], Hiroshi Furusho[1], Kenji Sakata[1], Eva Buys[2], Patrick Sips[2,5], Micah L. Burch[2], Yanbin Zhao[2], Amy E. Kelly[2], Masanobu Namura[6], Yoshihito Kita[7], Taketsugu Tsuchiya[8], Bunji Kaku[9], Kotaro Oe[10], Yuko Takeda[1], Tetsuo Konno[1], Masaru Inoue[11], Takashi Fujita[12], Takeshi Kato[1], Akira Funada[1], Hayato Tada[1], Akihiko Hodatsu[1], Chiaki Nakanishi[1], Yuichiro Sakamoto[13], Toyonobu Tsuda[1], Yoji Nagata[1], Yoshihiro Tanaka[1], Hirofumi Okada[1], Calum A MacRae[2], Seiji Takashima[14], Masakazu Yamagishi[1, 15], Masa-aki Kawashiri[1], and Masayuki Takamura[1].

[1]Department of Cardiology, Kanazawa University Graduate School of Medicine, Kanazawa, Japan; [2] Division of Cardiovascular Medicine, Department of Medicine, Brigham and Women's Hospital and Harvard Medical School, Boston, USA; [3]Department of Cardiovascular Medicine, Osaka University Graduate School of Medicine, Suita, Japan; [4]Department of Physiology, Kanazawa Medical University, Uchinada, Japan; [5]Center for Medical Genetics Ghent, Department of Pediatrics and Medical Genetics, Ghent University, Ghent, Belgium; [6]Department of Cardiology, Kanazawa Cardiovascular Hospital, Kanazawa, Japan; [7]Department of internal medicine, Wajima Municipal Hospital, Wajima, Japan; [8]Trans-catheter Cardiovascular Therapeutics, Kanazawa Medical University, Uchinada, Japan; [9]Division of Cardiovascular Medicine, Toyama Red Cross Hospital, Toyama, Japan; [10]Division of Internal Medicine, Saiseikai Kanazawa Hospital, Kanazawa, Japan; [11]Department of Cardiology, Ishikawa Prefectural Central Hospital, Kanazawa, Japan; [12]Division of Cardiology, Kouseiren Takaoka Hospital, Takaoka, Japan; [13]Division of Cardiology, Toyohashi Heart Center, Toyohashi, Japan; [14]Department of Medical Biochemistry, Osaka University Graduate School of Medicine, Suita, Japan; and [15]Osaka University of Human Sciences, Settu, Japan.

Short title: Pathogenic variants with cardiac conduction diseases

Address for correspondence:
Kenshi Hayashi, M.D., Ph.D.
Department of Cardiology, Kanazawa University Graduate School of Medicine,
13-1, Takara-machi, Kanazawa, Ishikawa 920-8641, Japan
Telephone: +81-76-265-2254
Fax: +81-76-234-4251
E-mail:kenshi@med.kanazawa-u.ac.jp

The category of the manuscript: Original article
The total word count: 6670
The contribution of each author to the study:
All authors contributed to the work described in the paper and all take responsibility for it. K. Hayashi, Y. Asano, M. Beerens, Y. Kurata, C. MacRae, S. Takashima, and M. Yamagishi designed the study. K. Hayashi, N. Fujino, H. Furusho, K. Sakata, M. Namura, Y. Kita, T. Tsuchiya, B. Kaku, K. Oe, Y. Takeda, T. Konno, M. Inoue , T. Fujita, T. Kato, A. Funada, H. Tada, A. Hodatsu, C. Nakanishi, Y. Sakamoto, T. Tsuda, Y. Nagata, Y. Tanaka, H. Okada, M. Kawashiri, and M. Takamura conducted cardiovascular screening, examination, and clinical follow up. K. Hayashi, R. Teramoto, Y. Asano, M. Beerens, Y. Kurata, E.Buys, P. Sips, M. Burch, Y. Zhao, A Kelly, and Y. Tanaka performed experiments and collected the data. K. Hayashi, A. Nomura, R. Teramoto, Y. Asano, and Y. Kurata analyzed the data. K. Hayashi, A. Nomura, R. Teramoto, Y. Asano, Y. Kurata and M. Yamagishi wrote the manuscript.

ABSTRACT

Aims: The genetic cause of cardiac conduction system disease (CCSD) has not been fully elucidated. Whole-exome sequencing (WES) enables the detection of a variety of genetic variants; however, the identification of pathogenic variants remains a challenge. We aimed to identify pathogenic or likely pathogenic variants in patients with CCSD by using WES and 2015 American College of Medical Genetics and Genomics (ACMG) standards and guidelines as well as evaluating the usefulness of functional studies for determining them.

Methods and Results: We performed WES of 23 probands diagnosed with early-onset (<65 years) CCSD and analyzed 117 genes linked to arrhythmogenic diseases or cardiomyopathies. We focused on rare variants (minor allele frequency < 0.5%) that were absent from the in-house WES data. We used 2015 ACMG standards and guidelines to classify these variants. Five probands had pathogenic variants in the *EMD* and *LMNA* genes. To evaluate the functional change of an *LMNA* c.339dupT, we sought to generate a knock-out zebrafish with CRISPR-mediated insertions or deletions of the human *LMNA* homolog, *lmna* in zebrafish. The mean heart rate and conduction velocities of the CRISPR/Cas9-injected embryos and F2 generation embryos with homozygous deletions were significantly decreased compared with those of the controls. Twenty-four variants of uncertain significance were identified in 14 probands. Cellular electrophysiological study showed that 3 variants in the *KCNA5*, *KCNH2*, and *SCN5A* genes, and 4 variants in the *SCN10A* genes damaged each gene, which resulted in the change of the clinical significance of these variants from “Uncertain significance” to “Likely pathogenic” in 5 probands.

Conclusions: Of 23 probands with CCSD, we successfully identified pathogenic or likely pathogenic variants in 10 probands (43%). Functional analyses of a cellular electrophysiological study and CRISPR/Cas9-mediated gene knock-out in zebrafish might be useful for determining the pathogenicity of rare variants in patients with CCSD.

Translational Perspective: Whole-exome sequencing (WES) may be helpful in determining the causes of cardiac conduction system disease (CCSD), however, the identification of pathogenic variants remains a challenge. We performed WES of 23 probands diagnosed with early-onset CCSD, and identified 12 pathogenic or likely pathogenic variants in 10 of these probands (43%) according to the 2015 ACMG standards and guidelines. In this context, functional analyses of a cellular electrophysiological study and CRISPR/Cas9-mediated gene knock-out in zebrafish might be useful for determining the pathogenicity of rare variants, and *SCN10A* may be one of the major development factors in CCSD.

1. Introduction

Bradyarrhythmia is a common clinical finding and can be usually due to a physiologic reaction, pharmacotherapy, or advanced age. Patients with bradyarrhythmia may present with syncope, symptoms of heart failure, and rarely sudden cardiac death. The cardiac conduction system consists of the sinus node, atrio-ventricular node, and His-Purkinje system. Bradyarrhythmia can be categorized on the level of disturbances in the hierarchy of this system and includes sinus node dysfunction and atrioventricular conduction disturbances or blocks.[1]

The pathophysiologic mechanisms underlying cardiac conduction-system disease (CCSD) are divided into acquired or inherited causes. Several studies showed genetic variants associated with CCSD linked to either structurally normal heart diseases (*HCN4, CACNA1G, CACNA1D, SCN5A, SCN1B, Cx40, KCNJ2, TRPM4, KCNK17, ANK2, CAV3, CASQ2,* and *RYR2* genes) or structural heart diseases (*MYH6, PRKAG2, Nkx2.5, Tbx5, LMNA, EMD, SGOL1*, and *LAMP-2* genes).[1-5] Thus, high-throughput sequencing (HTS) may be helpful in determining the causes of CCSD because of their comprehensiveness.[6, 7] However, few studies exist whether whole exome sequencing is useful for detecting causative variants in patients with early-onset CCSD.

Advancement of HTS has identified lots of putative variants associated with inherited cardiac disease. However, determining true pathogenicity of targeted diseases is still a major challenge.[8] In 2015, the American College of Medical Genetics and Genomics (ACMG), the Association for Molecular Pathology (AMP), and the College of American Pathologists reported updated standards and guidelines for the classification of sequence variants using criteria informed by expert opinion and empirical data.[9] This guideline consists of 28 criteria based on different sources of data including population data, computational and predictive data, functional data, segregation data, de novo data, and allelic data. Of these criteria, functional studies could be one of the powerful tools in support for disease pathogenicity.[9] The gold standard for the functional analysis of ion-channel variants is an electrophysiological measurement using a patch-clamp method in cell expression systems[10] and a simulation study with mathematical models of human cardiomyocytes. In addition, zebrafish is an emerging model for studying cardiac diseases, including cardiac arrhythmia.[11-16] Moreover, CRISPR/Cas9-mediated gene knock-out in zebrafish can facilitate high-throughput screens for phenotypic effects with high levels of on-target efficiency and relatively off-target modifications.[17, 18] However, in vivo zebrafish assay using CRISPR/Cas9 systems has not been fully established for interpreting pathogenicity of human rare variants associated with CCSD.

Here, we assessed 23 probands diagnosed with early-onset CCSD with pacemaker implantation (PMI) or a family history of PMI. We exome-sequenced for these patients to identify putative variants that could cause a CCSD. Then, we performed functional studies to re-classify guideline-based pathogenicity for these variants, using a patch-clamp method in heterologous expression systems, a simulation study, and the combination of CRISPR/Cas9 systems with zebrafish.

2. Methods

All data and supporting materials have been provided in the published article. An expanded Methods section is available in the Online Supplementary Data.

2.1 Study patients

The study conformed with the principles outlined in the Declaration of Helsinki and was approved by the Ethics Committee for Medical Research at our institution. All study patients provided written informed consent before registration.

The study patients were recruited from multiple hospitals in Japan. Early-onset CCSD was defined as bradyarrhythmia occurring in individuals aged <65 years, who showed an atrioventricular (AV) block and/or a sick sinus syndrome (SSS) with PMI or a family history of PMI as described in the Online Supplementary Data. In addition, we used DNA-sequencing data of 102 control subjects without electrocardiogram (ECG) abnormality.

2.2 DNA isolation and whole-exome DNA sequencing

WES was performed using the Illumina HiSeq platform (Illumina, San Diego, CA, USA) as described in the Online Supplementary Data. After the standard quality control, we selected only the variants that were absent in the in-house WES data from 102 control individuals without early-onset CCSD. Of those, we extracted the variants in 117 candidate genes linked to arrhythmogenic disorders or cardiomyopathy as a single gene disorder for further analyses (Supplemental Table 1).

2.3 Pathogenicity of candidate variants

We interpreted the sequence variants using 2015 ACMG standards and guidelines, which provided criteria for the classification of pathogenic or likely pathogenic variants.[9] Each pathogenic criterion is weighted as very strong (PVS1), strong (PS1–4), moderate (PM1–6), or supporting (PP1–5). Rare variants were defined as those with a minor allele frequency <0.5% in East Asians of the Human Genetic Variation Database (HGVD) version 2.3 and the Genome Aggregation Database (gnomAD) version 2.0.2. Variants that were absent from these databases were considered PM2. We selected protein-truncating variants (PTVs) in known genes associated with CCSD (PVS1), or rare missense variants registered as pathogenic or disease-causing mutations associated with CCSD in the ClinVar and Human Gene Mutation Database (HGMD) (PP5) All variants were annotated by the Variant Effect Predictor version 82 and referred following *in silico* damaging scores: MetaSVM for missense variants; LOFTEE for PTVs; and CADD for all variants.[19] CADD score of 15 indicated that the variant is predicted to be among the 15% most deleterious substitutions that can occur in the human genome. When multiple lines of these in silico prediction algorithms supported a deleterious effect on the gene, the supporting pathogenic evidence of PP3 was assigned. We further sought to determine the relationship between the clinical phenotype (bradyarrhythmia) and the genotype for probands and their relatives in whom a variant was identified (PP1 or PP4). These segregation analyses were performed in the family members as much as possible. If the missense variants are common causes of the disorder and the gene has very few benign variants, then a missense variant in this gene can be supporting evidence for pathogenicity (PP2). Functional studies used cellular electrophysiological analysis, mathematical modeling, and simulations, and CRISPR/Cas9 mediated gene knock-out in zebrafish to confirm the pathogenicity of the detected variants (PS3 or BS3). For a given variant, we selected the criteria based on the evidence observed

for the variant. The criteria are then combined according to the scoring rules to choose a classification from the 5-tier system.[9]

2.4 CRISPR-mediated deletions of the human *LMNA* ortholog, *lmna*, in zebrafish

All zebrafish experiments have been approved by Institutional Animal Care and Use Committee (protocol# BWH 2016N000276), which is certified by the Association for Assessment and Accreditation of Laboratory Animal Care. Zebrafish euthanasia was performed following NIH (https://oacu.oir.nih.gov/animal-research-advisory-committee-guidelines) and American Veterinary Medical Association guidelines using an overdose of Tricaine (M-222 or 3-aminobenzoic acid ethyl ester) in combination with hypothermic shock.

The gene editing in zebrafish with CRISPR/Cas9 was conducted to evaluate detected PTV in the *LMNA* gene from a patient with early-onset CCSD as described in the Online Supplementary Data.

Cardiac phenotypes were scored at 48 and 72 hpf, and genomic DNA was prepared from 10 individuals for Sanger sequencing as described in the Online Supplementary Data. The heart rate was visually counted at 48 hpf by using a stereomicroscope. Cardiac function was evaluated at 48 hpf by using video microscopy with an Axioplan (Zeiss) upright microscope. Voltage mapping was recorded on isolated 72 hpf zebrafish hearts.[20]

Mosaic founders (F0) were raised and were outcrossed to a wild-type line at the age of 3 months (Supplemental figure 1). Heterozygous F1 generation fishes with same *lmna* mutation were incrossed, and cardiac phenotypes for F2 embryos were evaluated as stated above. Each F2 embryo was genotyped after evaluation of the cardiac phenotype to distinguish between heterozygous and homozygous carriers.

2.5 Plasmid constructs and transfection of mammalian cell lines

Mutant cDNAs were constructed by an overlap extension strategy or using a QuikChange XL Site-Directed Mutagenesis Kit (Agilent Technologies, Santa Clara, CA, USA) as described in the Online Supplementary Data. Mammalian cells were transfected with the cDNA encoding potassium or sodium channels and green fluorescent protein (GFP) as described in the Online Supplementary Data. Cells displaying green fluorescence 48–72 h after transfection were subjected to electrophysiological analysis.

2.6 Electrophysiology and data analysis

Potassium or sodium currents were studied using the whole-cell patch clamp technique with an amplifier, Axopatch-200B (Molecular Devices, Sunnyvale, CA, USA), at room temperature as described in the Online Supplementary Data.

2.7 Mathematical modeling and simulations

With mathematical models of human ventricular myocytes[21] and rabbit peripheral sinoatrial node (SAN) cells,[22] effects of the changes in kinetic behavior of I_{Kr} and I_{Na} on the mid-myocardial action potential configuration of the ventricular myocyte model and pacemaker activity of the peripheral SAN cell model connected to the atrial membrane model via the gap junction conductance were evaluated. Dynamic behaviors of the model cell were determined by solving a system of nonlinear ordinary differential equations numerically. Numerical integration was performed on Workstation

HP xw9400 with MATLAB 7.5 (The MathWorks, Inc., Natick, MA, USA). The numerical algorithms available as a MATLAB ODE solver, *ode15s* (a variable time-step numerical differentiation approach selected for its suitability to stiff systems), were used.

2.8 Statistical analysis

Pooled electrophysiological data were expressed as mean ± standard error. Two-tailed Student's *t*-test was used for the single comparisons between the two groups. One-way analysis of variance, followed by a Bonferroni *post hoc* test, was used to analyze data with equal variance among three or more groups. A $P<0.05$ was considered statistically significant. Statistical analysis was performed using JMP Pro 11.0.0 (SAS Institute Inc., NC, USA) and Origin 2018 (OriginLab, Northampton, MA, USA).

3. Results

3.1 Clinical characteristics and molecular genetic analysis of the study cohort

The mean age of the study participants was 40 ± 16 years at the diagnosis of CCSD (Table 1). Of 23 subjects, 12 were women (52%), 13 had SSS (57%), and 17 (74%) had AV block in one first-degree relative, and 18 (78%) underwent PMI. Echocardiographic data revealed a normal mean ejection fraction. Atrial fibrillation (AF) and muscular disease were complicated in 12 (52%) and 2 (10%) subjects, respectively.

The genetic analysis showed that 5 PVS1 null variants were identified in the *EMD* and *LMNA* genes where loss of function is a known pathogenicity for CCSD (Table 2). These PTVs were absent from the controls in gnomAD or HGVD (PM2). Both CADD and LOFTEE indicated a deleterious effect of these PTVs on each gene (PP3) (Supplemental Table 2). ClinVar or HGMD classified *EMD* p. W226X, *LMNA* c. 1489-2A>G, and *LMNA* p. R321X into pathogenic, or disease causing variants (PP5). In addition to these 5 PTVs, 1 PTV and 14 missense variants were absent from the controls (PM2), 1PTV and 23 missense variants were considered as deleterious by in silico predictive algorithms (PP3), and 4 missense variants were classified as disease causing variants by HGMD (PP5) (Table 2 and Supplemental Table 2).

3.2 Clinical characteristics of patients with PTVs in the *EMD* or *LMNA* gene

We identified 2 PTVs in the *EMD* gene and 3 PTVs in the *LMNA* gene (Table 2). Two patients harboring PTVs in the *EMD* gene were diagnosed with CCSD at the age of 33 and 17 years, respectively. They showed AV block and AF in addition to muscular dystrophy, and underwent PMI[23] (Table 3). With regard to patient 1 with *EMD* p.W226X, we previously reported an Emery–Dreifuss muscular dystrophy (EDMD) family including 16 carriers (7 men and 9 women) with *EMD* p.W226X. EDMD caused by the *EMD* gene mutation is associated with X-linked recessive inheritance. All of the 7 male carriers had cardiac involvement, and their first cardiac manifestation occurred at age 10 to 37 years (mean age, 20.9 years) (PP1).[23] In patient 2, the segregation variant was confirmed in the *EMD* gene (p. Q222X). Proband's parents did not have this variant which was classified as de novo mutation (PS2).

Three patients harboring PTVs in the *LMNA* gene were diagnosed with CCSD at the age of 39, 23, and 44 years, respectively. Patient 3 with *LMNA* K114XfsX1 was a 55-year-old woman (Table 3). Her ECG showed first-degree AV block at age 39 years and sinus arrest at age 41 years. She had a family history of SCD and PMI. She received PMI at age 42 years and developed AF at 47 years. Echocardiogram showed low normal LV systolic function. Patient 4 with *LMNA* 1489-2A>G was a 23-year-old man (Table 3). His mother died suddenly due to ventricular fibrillation at the age of 50 years. His ECG showed AF and complete AV block, and received ICD therapy. Echocardiogram showed normal LV systolic function. Patient 5 with *LMNA* R321X was a 44-year-old woman (Table 3). She had a family history of SCD and PMI. Her ECG showed paroxysmal AF at age 32 years and first-degree AV block at age 43 years. She received ICD therapy at the age of 44 years old. Echocardiogram showed normal LV systolic function.

PTVs in the *EMD* and *LMNA* genes could be defined as pathogenic on the basis of "1 very strong (PVS1) and 1 Moderate (PM2) and 1 supporting by the guideline (PP1, PP3, or PP5) (Table 2).

3.3 Functional studies of PTV in the *LMNA* gene using zebrafish

We studied the usefulness of in vivo zebrafish assay using CRISPR/Cas9-mediated gene knock-out for

interpreting PTVs associated with CCSD. We sought to confirm the functional effect of one of PTVs, c. 339dupT, p. K114XfsX1 in the *LMNA* gene. The human *LMNA* homolog, *lmna*, in zebrafish is only one copy, and the percentage of the orthologous sequence matching the human sequence is 63.13%.

The target site was selected around the equivalent *lmna* site of the human *LMNA* c.339dupT (Figure 1A). Subsequently, sg RNA and Cas9 protein or only sg RNA was microinjected into one-cell stage zebrafish embryos. At 48 hpf after the microinjection, the appearance of both embryos looked similar (Supplemental Figure 2A). Genomic DNA was prepared from 10 individuals, and Sanger sequencing showed a variety of mutations in CRISPR/Cas9-injected embryos (Supplemental Figure 2A). At 48 hpf, the HR of zebrafish embryo was visually counted under upright microscope. The mean HR of the CRISPR/Cas9-injected embryos significantly decreased compared with those of CRISPR-only injected or non-injected embryos (Supplemental Figure 2B). Voltage mapping on isolated 72 hpf zebrafish hearts showed that the mean conduction velocities of the ventricle (mm/s) were significantly decreased in the CRISPR/Cas9-injected embryos compared with CRISPR-only injected embryos (8.0 ± 1.2 vs.16.8 ± 2.6; P<0.01) (Supplemental Figure 2C).

We also evaluated F2 zebrafish embryos. Sequencing analysis of F1 fish after outcross between mosaic founders (F0) and wild-type fishes showed various truncating indels. Of 10 genotyped F1 fish, 6 had heterozygous *lmna* c. 316_319 del GTGC, p. E108TfsX5, which caused a premature stop codon (1 male and 5 females). Cardiac phenotypes for F2 embryos after incross between these heterozygous fishes were evaluated. Subsequently, each F2 embryo was genotyped after evaluation of the cardiac phenotype to distinguish between heterozygous and homozygous carriers. The appearance of both embryos (*lmna* $^{+/+}$ and *lmna* $^{del/del}$) looked similar (Figure 1B). The mean HR of *lmna* $^{del/del}$ significantly decreased compared with those of *lmna* $^{+/+}$ (Figure 2A). The evaluation of cardiac function using video microscopy showed that the mean stroke volume, mean cardiac output, and the mean fractional area change of *lmna* $^{del/del}$ significantly increased compared with those of *lmna* $^{+/+}$ (Table 4 and Figure 2B). Voltage mapping on isolated 72 hpf zebrafish hearts showed that mean conduction velocities of both atrioventricular canal and ventricle were significantly decreased in *lmna* $^{del/del}$ compared with *lmna* $^{+/+}$. In contrast, those of atrium were comparable between these two groups (Table 4 and Figure 2C and D).

3.4 Clinical characteristics of a patient harboring both two rare missense variants in *KCNH2* and *SCN5A* and functional properties of the variants

Furthermore, we sought to define the functional effect of 2 rare missense variants classified as "uncertain significance" by the guideline in *KCNH2* and *SCN5A* genes.

Patient 7 with *SCN5A* P1824A and *KCNH2* R269W was a 47-year-old woman.[24] Her ECG showed SA block, AV block, and marked QT prolongation (HR 56/min, QTc 0.56 s). Holter ECG monitoring revealed a 4.5 seconds pause with transient loss of consciousness. She had a family history of PMI and considered to be an indication for PMI. Echocardiogram showed normal LV systolic function.

HEK293 cells were transiently transfected with vectors expressing wild-type or P1824A cDNA and the human beta1 subunit cDNA in combination with a bicistronic plasmid encoding GFP. Compared with the wild-type Nav1.5 channel, P1824A significantly reduced the peak sodium current density. The maximum peak current density of P1824A was −846 ± 131 pA/pF, which was significantly smaller than −1485 ± 186 pA/pF for wild-type (P<0.05) (Figures 3A, 3C and Table 5). No difference was found in persistent sodium current between wild-type (0.50% ± 0.07% of peak) and

P1824A (0.30% ± 0.07% of peak) (Figure 3B). The voltage dependence of steady-state activation of P1824A was significantly shifted in depolarizing (+ 5.7 mV) directions (Figure 3D and Table 5). No significant difference was observed in the voltage dependence of steady-state fast inactivation (Figure 3D).

Then, we transiently expressed Kv11.1 channels of wild-type, R269W, and wild-type + R269W in cultured mammalian CHO-K1 cells for whole-cell voltage clamp measurements (Figure 3E). Electrophysiological studies showed that the maximum tail current of R269W was 41.3 ± 7.4 pA/pF, which was significantly smaller than 84.2 ± 11.2 pA/pF for wild-type ($P<0.05$) (Figure 3F and Table 5). The maximum tail current of wild-type + R269W was 75.7 ± 18.7 pA/pF, which was comparable to that of wild-type alone. No significant difference in activation and deactivation kinetics was observed among three channels (Figures 3G and H, Table 5). The steady-state inactivation was shifted in its voltage dependence to a negative potential of −80.8 ± 8.6 mV for R269W and −63.0 ± 4.8 mV for wild-type + R269W compared with that of wild-type (−50.1 ± 4.5 mV) (R269W vs. wild-type, $P<0.05$) (Figure 3G and Table 5).

Simulation study showed that the mutational changes in the conductance and activation/deactivation/inactivation kinetics of I_{Kr} and I_{Na} prolonged the mid-myocardial action potential duration by 58% in the patient model of human ventricular myocytes and led to the formation of early afterdepolarizations when I_{Kr} was blocked by 7% (Figures 4A and B). The study also showed that I_{Na} and I_{Kr} during spontaneous action potentials of the patient peripheral SAN model were much smaller than those of the normal model (Figure 4C). Electrotonic modulations of the atrial myocyte caused arrhythmic dynamics (bradyarrhythmia) and cessation of pacemaker activity in the patient SAN model, but not in the normal one.

3.5 Clinical characteristics of a patient with rare PTV and missense variants in *SCN10A gene*, and electrophysiological studies for these variants.

Finally, we found one PTV and 5 rare missense variants classified as "uncertain significance" by the guideline in the *SCN10A* gene in 4 of 23 patients with CCSD (Table 3). Patient 6 with *SCN10A* R1263X showed paroxysmal AF at age 49 years and had a sinus pause of 3.6 s following termination of AF on his monitoring ECG at age 51 years. He received pacemaker therapy. He also had a rare variant, *KCNA5* T527M. We previously assessed the functional property of KCNA5 T527M channel.[10] Cellular electrophysiological studies showed that the activating current density for T527M was significantly larger than that for wild-type. The T527M mutant displayed a negative voltage shift in the normalized activation curve. Patient 8 with *SCN10A* I1482V was diagnosed as SSS, AV block, and AF at age 42 years. She received a pacemaker therapy at the age of 56 years old. Patient 9 with *SCN10A* D1819Y and M1373R had AV block at age 31 years. She developed syncope at age 36 years and received pacemaker therapy. Patient 10 with *SCN10A* F507L and G805S was a 17-year-old man who had SSS and received pacemaker therapy. Echocardiogram of these 4 patients showed normal LV systolic function.

ND7/23 cells were transiently transfected with vectors expressing wild-type, G805S, R1263X, M1373R, I1482V, or D1819Y *SCN10A* cDNA in the plasmid encoding GFP. Figure 5A shows representative current traces recorded for these wild-type and rare variant Nav 1.8 channels. Neither R1263X nor M1373R generated sodium currents, whereas wild-type, G805S, I1482V, and D1819Y generated sodium currents. Compared with the wild-type, G805S and D1819Y decreased the peak sodium current density, and I1482V increased the current density. The maximum peak

current density of I1482V was −162.9 ± 30.3 pA/pF, which was significantly larger than −101.0 ± 8.9 pA/pF for wild-type ($P<0.05$) (Figures 5A, B and Table 6). The voltage dependence of steady-state activation of I1482V was significantly shifted by 8.9 mV in hyperpolarizing directions (Figure 5C and Table 6). G805S variant caused a significant depolarizing shift (+ 4.5 mV) in the voltage-dependence of inactivation (Figure 5D and Table 6).

3.6 Classification of rare variants in consideration of functional studies

Above functional studies demonstrated that 8 rare variants in the *KCNA5*, *KCNH2*, *SCN5A*, *SCN10A*, and *LMNA* genes could have damaging effects on each target gene (PS3) (Table 2). Of those, 7 variants changed their clinical significance from “uncertain significance” to “likely pathogenic” when added the functional study results: “1 strong (PS3) and 1 Moderate (PM2)” or “1 strong (PS3) and 2 supporting (PP3 and PP5) (Table 2).

4. Discussion

In the present study, we analyzed 23 patients with CCSD for rare variants in arrhythmia and/or cardiomyopathy-related 117 genes using HTS. Since functional studies contributed greatly to the determination of the precise pathogenicity of variants of unknown significance, we finally determined 5 pathogenic variants in 5 patients and 7 likely pathogenic variants in 5 patients according to 2015 ACMG standards and guidelines.

This study provided some interesting findings. First, we identified 2 PTVs in the *EMD* gene and 3 PTVs in the *LMNA* gene as pathogenic. Also, we could confirm its pathogenicity by functional properties of one PTV in the *LMNA* gene using the CRISPR/Cas9-mediated zebrafish. The *EMD* and *LMNA* genes are known to be the disease-causing genes of EDMD with manifestation as high-grade AV block. The former is associated with X-linked recessive inheritance and the latter with autosomal dominant, autosomal recessive, and sporadic forms of EDMD. Both genes encode nuclear envelope proteins. EDMD is a genetically heterogeneous disorder characterized by early contractures, slowly progressive muscle wasting and weakness, and cardiomyopathy with conduction block. Some patients present with conduction disturbances or atrial cardiomyopathy even when skeletal myopathy is absent and are possible candidates for these mutations. In terms of CRISPR/Cas9-mediated zebrafish analysis, it has been used as a useful in vivo model to assay the pathogenicity of human variants in familial cardiovascular diseases.[25-27] Zebrafish has the advantage of transparency, low cost, and the ability to manipulate their genome efficiently. Zebrafish can gain a prominent role as the models of thousands of candidate disease-associated genes and alleles.[28] The recent sequencing of zebrafish revealed that approximately 70% of human genes had functional homologs in zebrafish.[28] We confirmed that the human *LMNA* homolog, *lmna*, in zebrafish is only one copy, and the percentage of the orthologous sequence matching the human sequence was 63.13%. Namely, human pathogenesis of CCSD with the *LMNA* gene mutation could be modeled in zebrafish.

Second, we could determine the pathogenicity of 7 rare ion channel variants with previously defined as “unknown significance” by two functional analyses, electrophysiological and simulation studies. *SCN5A* P1824A and *KCNH2* R269W were identified from the proband with SSS, AV block, and QT prolongation.[24] Electrophysiological study demonstrated that both mutations showed loss-of -function. A simulation study demonstrated that *SCN5A* P1824A might contribute to sinus node dysfunction. The *SCN5A* gene encodes for the α-subunits of the voltage-gated Na^+ channels (the Nav 1.5 channel), which is expressed in the conduction system and in the atrial regions surrounding the SAN and the atrio-ventricular node.[29] In contrast, *KCNH2* variant might contribute to both sinus node dysfunction and QT prolongation as clinical phenotype expressions. The simulation study was useful in explaining the role of each variant in multiple disorders. *KCNA5* T527M was identified from the proband with SSS and AF. We previously reported that T527M showed a gain-of-function effect with an enhanced steady-state activation, which could result in susceptibility to AF and a sinus pause after the termination of AF.[10] However, this variant is present at a relatively high frequency in East Asians which suggests either very low penetrance or only a modifying effect. This proband also had likely pathogenic variant, *SCN10A* R1263X which showed loss of function of Nav 1.8 channel and may be associated with proband’s phenotype

Third, we determined 4 likely pathogenic variants in 4 of 23 (17%) CCSD patients in the *SCN10A* gene. A cellular electrophysiological study demonstrated that three variants (G805S, R1263X and M1373R) showed loss-of-function effects, and one variant (I1482V) showed gain-of-

function effect. The voltage-gated sodium channel alpha subunit, Nav1.8 is encoded by the *SCN10A* gene and is highly expressed in sensory neurons of dorsal root ganglia. Several genome-wide association studies showed that *SCN10A* was associated with cardiac conduction. A recent review showed how *SCN10A* variants promote dysfunctional conduction: the cardiomyocyte, enhancer, and neuronal hypotheses.[30] CCSD caused by gain-of-function *SCN10A* rare variants may be explained through the neuronal hypothesis. The neuronal hypothesis stipulates that *SCN10A* indirectly exerts an effect on cardiac conduction through intracardiac neurons. SCN10A functions in cholinergic neurons to exert negative chronotropic and dromotropic effects on sinus and AV nodal tissues and modulates myocyte refractoriness. Gain-of-function *SCN10A* rare variants might cause vagus nerve stimulation and cardiac conduction disturbance. In contrast, the mechanism of causing CCSD by *SCN10A* loss-of-function rare variants is poorly understood. One possibility is that the enhancer hypothesis may be associated with the onset of CCSD by these variants. The enhancer hypothesis states that the cardiac enhancer located in *Scn10a* interacted with the promoter of *Scn5a* and was essential for *Scn5a* expression in murine cardiac tissue. Further studies are needed to clarify the mechanism by which loss-of-function *SCN10A* rare variants modulate cardiac conduction and lead to development of bradycardia.

This study has several limitations. First, only 117 genes linked to arrhythmogenic diseases or cardiomyopathies were examined for rare variants associated with CCSD. Causative genes may be included in the remaining genes other than these 117 genes. Second, of 13 probands with family history, familial aggregation and segregation analysis were performed only for two families with PTVs in the *EMD* gene. However, we evaluated pathogenicity of rare variants by functional studies, including a patch-clamp method, a simulation study, and the CRISPR-mediated deletions of the *lmna* in zebrafish. Third, approximately 30% of human genes did not have functional homologs in zebrafish. Actually, we could not find a human *EMD* homolog in zebrafish and did not evaluate the functional change of an *EMD* protein-truncating variant using zebrafish model. In addition, functional properties of most missense variants in non-ion-channel genes were not evaluated in this study.

5. Conclusions

Integrated HTS targeting 117 arrhythmia and cardiomyopathy-related genes with one-by-one various functional studies, we identified 12 pathogenic or likely pathogenic variants in 10 of 23 CCSD probands (43%): 5 probands harboring 5 pathogenic variants in genes encoding nuclear envelope proteins; 5 probands had at least one likely pathogenic variant in genes encoding ion channels. Notably, *SCN10A* may be one of the major development factors in CCSD.

Supplementary material

Supplementary material is available at *Cardiovascular Research* online.

Acknowledgments

The authors gratefully acknowledge Takako Obayashi, Hitomi Oikawa, and Amy Kelly for technical assistance.

Funding

This study was supported by grants from Grant-in-Aid for Scientific Research (C) Grant Number 26460670 and Fund for the Promotion of Joint International Research Grant Number 15KK0302 (K.H.), Takeda Science Foundation (K.H.), SENSHIN Medical Research Foundation (K.H.), and Suzuken Memorial Foundation (K.H.).

Conflict of interest

None declared

References

1. Beinart R, Ruskin J, Milan D. The genetics of conduction disease. *Heart Fail Clin*. 2010;**6**:201-214.
2. Wolf CM, Berul CI. Inherited conduction system abnormalities--one group of diseases, many genes. *J Cardiovasc Electrophysiol*. 2006;**17**:446-455.
3. Baruteau AE, Probst V, Abriel H. Inherited progressive cardiac conduction disorders. *Curr Opin Cardiol*. 2015;**30**:33-39.
4. Ishikawa T, Tsuji Y, Makita N. Inherited bradyarrhythmia: A diverse genetic background. *J Arrhythm*. 2016;**32**:352-358.
5. Rezazadeh S, Duff HJ. Genetic Determinants of Hereditary Bradyarrhythmias: A Contemporary Review of a Diverse Group of Disorders. *Can J Cardiol*. 2017;**33**:758-767.
6. Tan ZP, Xie L, Deng Y, Chen JL, Zhang WZ, Wang J, Yang JF, Yang YF. Whole-exome sequencing identifies Y1495X of SCN5A to be associated with familial conduction disease and sudden death. *Sci Rep*. 2014;**4**:5616.
7. Celestino-Soper PB, Doytchinova A, Steiner HA, Uradu A, Lynnes TC, Groh WJ, Miller JM, Lin H, Gao H, Wang Z, Liu Y, Chen PS, Vatta M. Evaluation of the Genetic Basis of Familial Aggregation of Pacemaker Implantation by a Large Next Generation Sequencing Panel. *PLoS One*. 2015;**10**:e0143588.
8. Ho CY, Charron P, Richard P, Girolami F, Van Spaendonck-Zwarts KY, Pinto Y. Genetic advances in sarcomeric cardiomyopathies: state of the art. *Cardiovasc Res*. 2015;**105**:397-408.
9. Richards S, Aziz N, Bale S, Bick D, Das S, Gastier-Foster J, Grody WW, Hegde M, Lyon E, Spector E, Voelkerding K, Rehm HL, Committee ALQA. Standards and guidelines for the interpretation of sequence variants: a joint consensus recommendation of the American College of Medical Genetics and Genomics and the Association for Molecular Pathology. *Genet Med*. 2015;**17**:405-424.
10. Hayashi K, Konno T, Tada H, Tani S, Liu L, Fujino N, Nohara A, Hodatsu A, Tsuda T, Tanaka Y, Kawashiri MA, Ino H, Makita N, Yamagishi M. Functional Characterization of Rare Variants Implicated in Susceptibility to Lone Atrial Fibrillation. *Circ Arrhythm Electrophysiol*. 2015;**8**:1095-1104.
11. Milan DJ, Macrae CA. Zebrafish genetic models for arrhythmia. *Prog Biophys Mol Biol*. 2008;**98**:301-308.
12. Sabeh MK, Kekhia H, Macrae CA. Optical mapping in the developing zebrafish heart. *Pediatr Cardiol*. 2012;**33**:916-922.
13. Wilkinson RN, Jopling C, van Eeden FJ. Zebrafish as a model of cardiac disease. *Prog Mol Biol Transl Sci*. 2014;**124**:65-91.
14. Vornanen M, Hassinen M. Zebrafish heart as a model for human cardiac electrophysiology. *Channels (Austin)*. 2016;**10**:101-110.
15. Kithcart A, MacRae CA. Using Zebrafish for High-Throughput Screening of Novel Cardiovascular Drugs. *JACC Basic Transl Sci*. 2017;**2**:1-12.
16. MacRae CA, Peterson RT. Zebrafish as tools for drug discovery. *Nat Rev Drug Discov*. 2015;**14**:721-731.
17. Gagnon JA, Valen E, Thyme SB, Huang P, Akhmetova L, Pauli A, Montague TG, Zimmerman S, Richter C, Schier AF. Efficient mutagenesis by Cas9 protein-mediated oligonucleotide insertion and large-scale assessment of single-guide RNAs. *PLoS One*. 2014;**9**:e98186.
18. Liu J, Zhou Y, Qi X, Chen J, Chen W, Qiu G, Wu Z, Wu N. CRISPR/Cas9 in zebrafish: an efficient combination for human genetic diseases modeling. *Hum Genet*. 2017;**136**:1-12.
19. McLaren W, Pritchard B, Rios D, Chen Y, Flicek P, Cunningham F. Deriving the consequences of genomic variants with the Ensembl API and SNP Effect Predictor. *Bioinformatics*. 2010;**26**:2069-2070.
20. Panakova D, Werdich AA, Macrae CA. Wnt11 patterns a myocardial electrical gradient through

regulation of the L-type Ca(2+) channel. *Nature*. 2010;**466**:874-878.
21. Kurata Y, Hisatome I, Matsuda H, Shibamoto T. Dynamical mechanisms of pacemaker generation in IK1-downregulated human ventricular myocytes: insights from bifurcation analyses of a mathematical model. *Biophys J*. 2005;**89**:2865-2887.
22. Kurata Y, Matsuda H, Hisatome I, Shibamoto T. Regional difference in dynamical property of sinoatrial node pacemaking: role of na+ channel current. *Biophys J*. 2008;**95**:951-977.
23. Sakata K, Shimizu M, Ino H, Yamaguchi M, Terai H, Fujino N, Hayashi K, Kaneda T, Inoue M, Oda Y, Fujita T, Kaku B, Kanaya H, Mabuchi H. High incidence of sudden cardiac death with conduction disturbances and atrial cardiomyopathy caused by a nonsense mutation in the STA gene. *Circulation*. 2005;**111**:3352-3358.
24. Itoh H, Shimizu W, Hayashi K, Yamagata K, Sakaguchi T, Ohno S, Makiyama T, Akao M, Ai T, Noda T, Miyazaki A, Miyamoto Y, Yamagishi M, Kamakura S, Horie M. Long QT syndrome with compound mutations is associated with a more severe phenotype: a Japanese multicenter study. *Heart Rhythm*. 2010;**7**:1411-1418.
25. Hodatsu A, Konno T, Hayashi K, Funada A, Fujita T, Nagata Y, Fujino N, Kawashiri MA, Yamagishi M. Compound heterozygosity deteriorates phenotypes of hypertrophic cardiomyopathy with founder MYBPC3 mutation: evidence from patients and zebrafish models. *Am J Physiol Heart Circ Physiol*. 2014;**307**:H1594-1604.
26. Jou CJ, Barnett SM, Bian JT, Weng HC, Sheng X, Tristani-Firouzi M. An in vivo cardiac assay to determine the functional consequences of putative long QT syndrome mutations. *Circ Res*. 2013;**112**:826-830.
27. Jou CJ, Arrington CB, Barnett S, Shen J, Cho S, Sheng X, McCullagh PC, Bowles NE, Pribble CM, Saarel EV, Pilcher TA, Etheridge SP, Tristani-Firouzi M. A Functional Assay for Sick Sinus Syndrome Genetic Variants. *Cell Physiol Biochem*. 2017;**42**:2021-2029.
28. Davis EE, Frangakis S, Katsanis N. Interpreting human genetic variation with in vivo zebrafish assays. *Biochim Biophys Acta*. 2014;**1842**:1960-1970.
29. Monfredi O, Dobrzynski H, Mondal T, Boyett MR, Morris GM. The anatomy and physiology of the sinoatrial node--a contemporary review. *Pacing Clin Electrophysiol*. 2010;**33**:1392-1406.
30. Park DS, Fishman GI. Nav-igating through a complex landscape: SCN10A and cardiac conduction. *J Clin Invest*. 2014;**124**:1460-1462.

Figure Legends

Figure 1 Appearance and base sequence of F2 generation zebrafish embryo with *lmna* deletion mutation.

(A) Multiple sequence alignment of human *LMNA* gene and zebrafish *lmna* gene. (B) Representative images illustrating the morphology of 2 dpf wild-type and *lmna*$^{del/del}$ mutants and Sanger sequence of *lmna* gene. DSB, double-strand break; PAM, protospacer adjacent motif

Figure 2 Functional studies of F2 zebrafish embryos with *lmna* deletion mutation.

(A) Heart rate of *lmna*$^{+/+}$ (n=15) and *lmna*$^{del/del}$ mutants (n=37). (B) Cardiac output of *lmna*$^{+/+}$ (n=15) and *lmna*$^{del/del}$ mutants (n=37). (C) Isochronal map of *lmna*$^{+/+}$ and *lmna*$^{del/del}$ mutants summarizing the regional spread of electrical activity across the atrium and into the ventricle. The lines represent the positions of the action potential wavefront at 5-ms intervals. The color scale depicts the timing of electrical activation (blue areas activated before red areas). (D) Mean estimated conduction velocities at the atrium, AV canal, and ventricle of *lmna*$^{+/+}$ (n=7) and *lmna*$^{del/del}$ mutants (n=9). Regions of interest was placed at middle of atrium, AV canal or ventricle. $^{\dagger}p<0.01$ vs. *lmna*$^{+/+}$ by two-tailed Student's t-test.

Figure 3 Functional properties of $Na_v1.5$ channel and $K_v11.1$ channel in a patient with *SCN5A* P1824A and *KCNH2* R269W.

(A) The voltage protocol and representative whole-cell Na^+ currents of the wild-type and P1824A $Na_v1.5$ channels. (B) Comparison of late Na^+ currents. The late Na^+ currents were measured at the end of 200-ms depolarizing pulses, as shown in the inset. (C) I–V relationships for peak currents in HEK293 cells transfected with wild-type (n=23) and P1824A (n=21). *p<0.05 vs wild-type by two-tailed Student's t-test. (D) The voltage protocols and the voltage dependence of steady-state fast inactivation and activation for wild-type (n=19 and 23) and P1824A (n=14 and 21). (E) The voltage protocol and representative expressed currents in CHO-K1 cells transfected with $K_v11.1$ wild-type alone, $K_v11.1$ R269W, and wild-type plus R269W. (F) I–V relationships for tail currents in CHO-K1 cells transfected with wild-type alone (closed circle, n=19), R269W (closed square, n=17), and wild-type plus R269W (closed triangle, n=12). *p<0.05 vs. wild-type by one-way ANOVA, followed by a Bonferroni *post hoc* test. (G) The voltage protocols and normalized steady-state activation and inactivation curves for wild-type alone (n=19, and 7), R269W (n=17 and 10), and wild-type plus R269W (n=12 and 9). (H) The voltage protocol and fast and slow components of deactivation time constants as a function of test potentials for wild-type alone (n=17), R269W (n=19), and wild-type plus R269W (n=21). The deactivation process was fit to biexponential functions.

Figure 4 Computer simulation of the effects of modified kinetic behavior of $K_v11.1$ and $Na_v1.5$ currents on electrophysiological properties of human ventricular myocytes (mid-myocardial cells) and the electrotonic effects of atrial myocytes on pacemaker activity of peripheral sinoatrial node (SAN) cells in a normal subject and a patient with modified $K_v11.1$ and $Na_v1.5$ currents.

(A) Simulated action potentials (top) and the time course of I_{Kr} during action potentials (bottom) of ventricular mid-myocardial cell models for a normal subject and a patient with modified $K_v11.1$ and $Na_v1.5$ currents. The model cells were paced at 1 Hz by 1-ms stimuli of 60 pA/pF for 10 min; steady-state behaviors after the last stimulus are shown. Modified inactivation/deactivation kinetics of KCNH2 R269W and SCN5A P1824A prolonged APD_{90} from 424.2 to 674.2 ms. (B) Simulated effects of I_{Kr} block on action potentials of ventricular mid-myocardial cells in the normal subject (top) and patient (bottom). Model cells with various I_{Kr} conductance (g_{Kr}) were paced at 0.5 Hz by 1-ms stimuli of 60 pA/pF for 10 min; steady-state behaviors after the last stimulus are shown. In the normal model with wild-type channels (top), 40% reduction of I_{Kr} only slightly prolonged APD_{90} from 467.3 to 534.4 ms. In contrast, in the patient model with mutant channels (bottom), only 7% reduction of I_{Kr} dramatically prolonged APD_{90} from 651.6 to 1177.5 ms and evoked early afterdepolarization. (C) Simulated spontaneous action potentials and time courses of I_{Na} and I_{Kr} in

SAN cell models for the normal subject (left) and patient (right). A peripheral SAN model cell was connected to two atrial cells with gap junction conductance (GJC) of 0–5 nS, as described previously[23]. I_{Na} and I_{Kr} during spontaneous action potentials of the patient model with mutant channels are much smaller than those of the normal model. In the normal model, increasing GJC (up to 5 nS), although slowing pacemaking, did not cause arrhythmic dynamics or cessation of spontaneous activity. In contrast, in the patient model, increasing GJC caused arrhythmic dynamics (skipped beat runs) at 4 nS and cessation of pacemaker activity at 5 nS.

Figure 5 The functional consequence of five variants in the *SCN10A* gene assessed by whole-cell patch clamp recording

(A) The voltage protocol and representative current traces of Na_v 1.8 using wild-type and mutant channels. (B) I–V relationships for peak currents in ND 7/23 cells transfected with *SCN10A* wild-type (n=64) and five variants including G805S (n=15), R1263X (n=15), M1373R (n=19), I1482V (n=25), and D1819Y (n=24). *$p<0.05$ or $^{\dagger}p<0.01$ vs. wild-type by one-way ANOVA, followed by a Bonferroni *post hoc* test. (C) Normalized steady-state activation curves of *SCN10A* wild-type (n=64), and three variants including G805S (n=15), I1482V (n=25), and D1819Y (n=24). (D) The voltage protocols and normalized steady-state inactivation curves of *SCN10A* wild-type (n=33) and three variants including G805S (n=13), I1482V (n=23), and D1819Y (n=22).

Table 1 Clinical characteristics of patients with early-onset cardiac conduction system diseases

Number of probands	23
Female (%)	12 (52)
Age at diagnosis (years)	40 ± 16
HR (bpm)	44 ± 12
Sick sinus syndrome (%)	13 (57)
R-S I/R-S II/R-S III	4/7/2
Atrioventricular block (%)	17 (74)
I/II/III	2/5/10
Family history of PMI	13 (57)
PMI (%)	18 (78)
Atrial fibrillation	12 (52)
LVEF (%)	66 ± 10
Muscular dystrophy	2 (10)

HR, heart rate; R-S, Rubenstein;
PMI, pacemaker implantation;
LVEF, left ventricular ejection fraction

Table 2

Table 2 Pathogenic or likely pathogenic variants determined by 2015 ACMG standards and guidelines

Gene	Base change	Amino acid change	PVS1	PS2	PS3	PM2	PP1	PP3	PP5	BS3	Classification without PS3 (functional studies)	Classification with PS3 (functional studies)	Patient number
EMD	677 G>A	W226X	✓			✓	✓	✓	✓		Pathogenic	Pathogenic	1
	664C>T	Q222X	✓	✓		✓		✓			Pathogenic	Pathogenic	2
LMNA	339dupT	K114XfsX1	✓		✓	✓		✓			Pathogenic	Pathogenic	3
	1489-2A>G		✓			✓		✓	✓		Pathogenic	Pathogenic	4
	961C>T	R321X	✓			✓		✓	✓		Pathogenic	Pathogenic	5
KCNA5	1580C>T	T527M			✓			✓	✓		Uncertain significance	Likely pathogenic	6
KCNH2	805C>T	R269W			✓	✓		✓	✓		Uncertain significance	Likely pathogenic	7
SCN5A	5470C>G	P1824A			✓	✓		✓	✓		Uncertain significance	Likely pathogenic	7
HCN4	2845C>T	R949W						✓			Uncertain significance	Uncertain significance	4
SCN10A	3787C>T	R1263X			✓	✓		✓			Uncertain significance	Likely pathogenic	6
	4444A>G	I1482V			✓	✓		✓			Uncertain significance	Likely pathogenic	8
	5455G>T	D1819Y				✓		✓		✓	Uncertain significance	Uncertain significance	9
	4118T>G	M1373R			✓	✓		✓			Uncertain significance	Likely pathogenic	9
	1519T>C	F507L				✓		✓			Uncertain significance	Uncertain significance	10
	2413G>A	G805S			✓	✓		✓			Uncertain significance	Likely pathogenic	10
RYR2	2300C>G	S767W						✓			Uncertain significance	Uncertain significance	11
MYH6	3347G>A	R1116H						✓			Uncertain significance	Uncertain significance	12
	3755G>A	R1252Q				✓		✓			Uncertain significance	Uncertain significance	12
MYH7	968T>C	I323T				✓		✓			Uncertain significance	Uncertain significance	10
MYH11	4532G>A	R1511Q				✓		✓			Uncertain significance	Uncertain significance	3
RBM20	3545G>A	R1182H						✓	✓		Uncertain significance	Uncertain significance	13
	3649G>A	G1217R						✓			Uncertain significance	Uncertain significance	6
TTN	70264G>C	G23422R						✓			Uncertain significance	Uncertain significance	14
DES	556G>A	D186N				✓		✓			Uncertain significance	Uncertain significance	14
CBS	1552T>C	Y518H				✓		✓			Uncertain significance	Uncertain significance	4
TBX5	409G>A	V137M						✓			Uncertain significance	Uncertain significance	7

ACTC1	710C>T	S237F	✓	✓	Uncertain significance	Uncertain significance	8
PRKAG2	1366C>G	R456G		✓	Uncertain significance	Uncertain significance	13
MAP2K2	937C>T	R313W	✓	✓	Uncertain significance	Uncertain significance	3

PVS1: null variant (nonsense, frameshift, canonical ±1 or 2 splice sites, initiation codon, single or multiexon deletion) in a gene where LOF is a known mechanism of disease.
PS2: De novo (both maternity and paternity confirmed) in a patient with the disease and no family history.
PS3: Well-established in vitro or in vivo functional studies supportive of a damaging effect on the gene or gene product.
PM2: Absent from controls (or at extremely low frequency if recessive) in Exome Sequencing Project, 1000 Genomes Project, or Exome Aggregation Consortium.
PP1: Cosegregation with disease in multiple affected family members in a gene definitively known to cause the disease.
PP3: Multiple lines of computational evidence support a deleterious effect on the gene or gene product.
PP5: Reputable source recently reports variant as pathogenic, but the evidence is not available to the laboratory to perform an independent evaluation.
BS3: Well-established in vitro or in vivo functional studies show no damaging effect on protein function or splicing.

ACMG, the American College of Medical Genetics and Genomics; AMP, the Association for Molecular Pathology; CAP, the College of American Pathologists; NA, not available; D, rare damaging variants; DM, disease causing mutation; EDMD, Emery-Dreifuss muscular dystrophy; DCM, dilated cardiomyopathy, AF, atrial fibrillation; LQTS, long QT syndrome, HCM, hypertrophic cardiomyopathy; VUS, variant of unknown significance.

Table 3

Table 3 Summary of clinical characteristics and detected rare mutations of patients with early-onset CCSD

Patient number	Gender	Age at diagnosis (yrs.)	SSS	AV block	FH of PMI	PMI	AF	LVEF (%)	Rare variants	Classification with PS3 (functional studies)
1	Male	33	—	✓	✓	✓	✓	53	*EMD* W226X	Pathogenic
2	Male	17	—	✓	—	✓	✓	60	*EMD* Q222X	Pathogenic
3	Female	39	✓	✓	✓	✓	✓	58	*LMNA* K114XfsX1 *MAP2K2* R313W *MYH11* R1511Q	Pathogenic
4	Male	23	✓	✓	✓	✓	✓	64	*LMNA* 1489-2A>G *CBS* Y518H *HCN4* R949W	Pathogenic
5	Female	44	—	✓	✓	✓	✓	61	*LMNA* R321X	Pathogenic
6	Male	51	✓	—	—	✓	✓	70	*KCNA5* T527M *SCN10A* R1263X *RBM20* G1217R	Likely pathogenic Likely pathogenic
7	Female	47	✓	✓	✓	✓	—	77	*SCN5A* P1824A *KCNH2* R269W *TBX5* V137M	Likely pathogenic Likely pathogenic
8	Female	42	✓	✓	✓	✓	✓	79	*SCN10A* I1482V *ACTC1* S237F	Likely pathogenic
9	Female	31	—	✓	—	✓	—	76	*SCN10A* D1819Y *SCN10A* M1373R	Likely pathogenic
10	Male	17	✓	—	—	✓	—	60	*SCN10A* F507L *SCN10A* G805S *MYH7* I323T	Likely pathogenic

CCSD, cardiac conduction system diseases; SSS, sick sinus syndrome; AV block, atrioventricular block; FH, family history; PMI, pacemaker implantation; AF atrial fibrillation; LVEF, left ventricular ejection fraction; underlined and bold rare variants indicate pathogenic variants.

Table 4 The evaluation of cardiac function at 48 hpf and conduction velocity at 72 hpf of the F2 embryos

	lmna $^{+/+}$	*lmna* $^{del/del}$
Cardiac function	n=15	n=37
HR (bpm)	145 ± 11	127 ± 15†
Stroke volume (nl)	0.39 ± 0.18	0.59 ± 0.15†
Cardiac output (nl/min)	54.97 ± 22.85	74.35 ± 19.70†
Fractional area change (%)	26.88 ± 8.72	38.87 ± 9.26†
Conduction velocity	n=7	n=9
Atrium (mm/sec)	3.86 ± 0.64	3.07 ± 0.30
Atrioventricular canal (mm/sec)	0.75 ± 0.12	0.40 ± 0.02†
Ventricle (mm/sec)	7.99 ± 0.81	4.23 ± 0.68†

†P<0.01 vs. *lmna*

Table 5 Biophysical properties of wild-type and P1824A Nav1.5 channels, and wild-type and R269W Kv11.1 channels

		Nav1.5		Kv11.1		
		Wild-type	P1824A	Wild-type	R269W	Wild-type /R269W
Cells (n)		23	21	19	17	12
Peak I_{Na} (pA/pF)		-1485 ± 186	-846 ± 131*	—	—	—
The maximum tail current (pA/pF)		—	—	84.2 ± 11.2	41.3 ± 7.4*	75.7 ± 18.7
Activation	$V_{1/2}$ (mV)	-49.5 ± 1.1	-43.8 ± 1.7*	3.8 ± 1.8	0.5 ± 2.3	3.9 ± 2.1
	SF (mV)	1.8 ± 0.2	3.4 ± 0.5*	7.9 ± 0.3	8.7 ± 0.4	8.5 ± 0.4
Cells (n)		19	14	7	10	9
Inactivation	$V_{1/2}$ (mV)	-75.9 ± 1.2	-76.6 ± 1.9	-50.1 ± 4.5	-80.8 ± 8.6*	-63.0 ± 4.8
	SF (mV)	5.1 ± 0.1	5.4 ± 0.1	20.9 ± 1.9	21.7 ± 1.7	19.7± 0.7
Cells (n)		—	—	17	19	21
Deactivation	$\tau_{fast, -80}$ (ms)	—	—	83.4 ± 10.6	162.3 ± 32.8	121.0 ± 16.2
	$\tau_{slow, -80}$ (ms)	—	—	514.0 ± 58.4	907.6 ± 166.2	747.0 ± 163.1

SF, Slope factor; *P<0.05 vs. wild-type

Table 6 Biophysical properties of wild-type, G805S, R1263X, M1373R, I1482V, and D1819Y Nav1.8 channels

		Wild-type	G805S	R1263X	M1373R	I1482V	D1819Y
Cells (n)		64	15	15	19	25	24
Peak I_{Na} (pA/pF)		-101.0 ± 8.9	-49.2 ± 9.5	-4.5 ± 0.4*	-4.8 ± 0.5*	-162.9 ± 30.3†	-63.3± 9.9
Activation	$V_{1/2}$ (mV)	9.8 ± 2.3	16.2 ± 3.8	—	—	0.9 ± 3.0*	12.2 ± 3.0
	SF (mV)	-8.9 ± 0.3	-8.7 ± 0.4	—	—	-8.2 ± 0.4	-9.6 ± 0.4
Cells (n)		33	13			23	22
Inactivation	$V_{1/2}$ (mV)	-71.7 ± 1.0	-67.2 ± 1.1*	—	—	-70.2 ± 1.2	-71.6 ± 1.7
	SF (mV)	10.0 ± 0.3	9.6 ± 0.4	—	—	9.2 ± 0.3	9.5 ± 0.3

SF, Slope factor; *P<0.05 vs. wild-type; †P<0.01 vs. wild-type

Figure 1

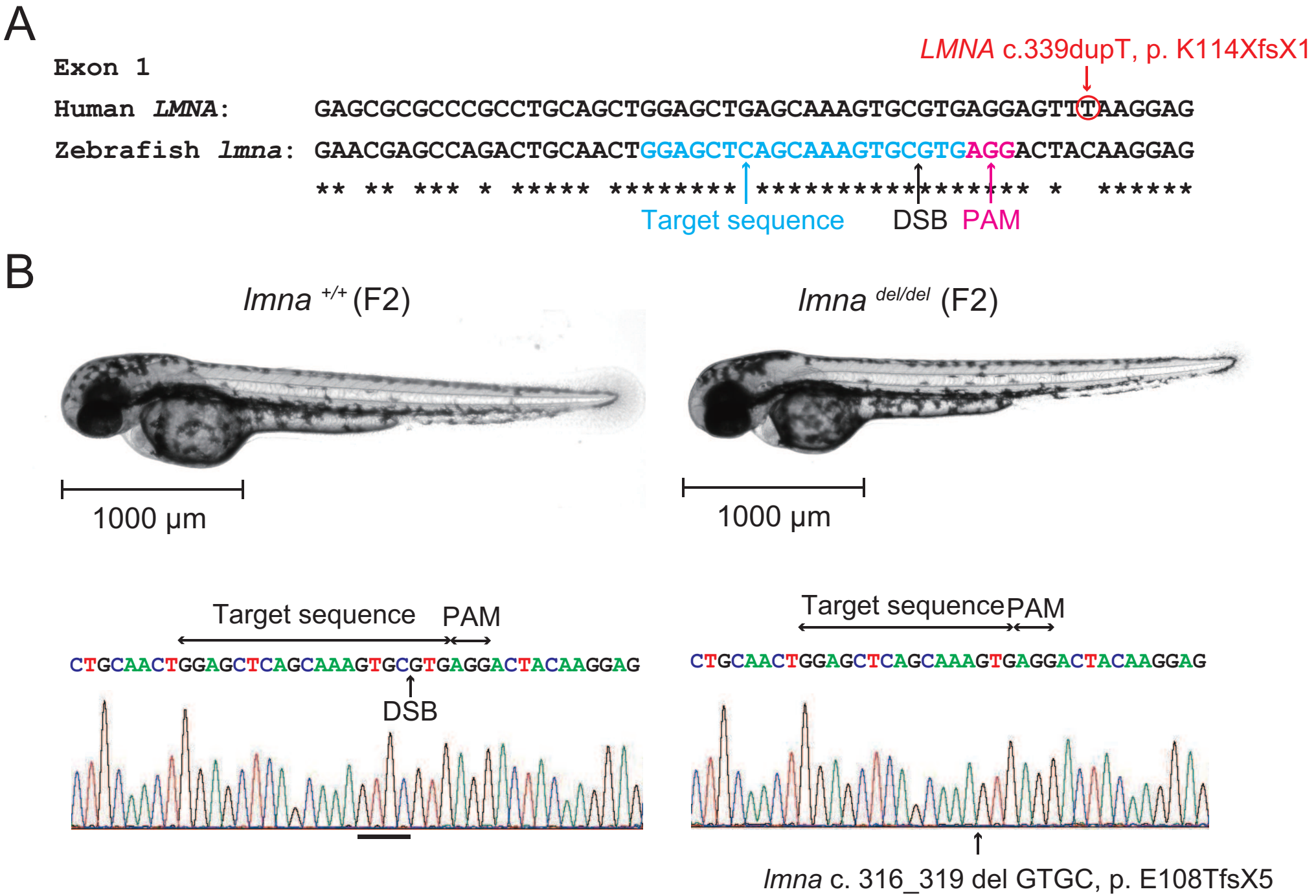
A
Exon 1
LMNA c.339dupT, p. K114XfsX1
Human LMNA: GAGCGCGCCCGCCTGCAGCTGGAGCTGAGCAAAGTGCGTGAGGAGTTTAAGGAG
Zebrafish lmna: GAACGAGCCAGACTGCAACTGGAGCTCAGCAAAGTGCGTGAGGACTACAAGGAG
Target sequence
DSB
PAM
B
lmna +/+ (F2)
lmna del/del (F2)
1000 µm
1000 µm
Target sequence
PAM
CTGCAACTGGAGCTCAGCAAAGTGCGTGAGGACTACAAGGAG
DSB
Target sequence
PAM
CTGCAACTGGAGCTCAGCAAAGTGAGGACTACAAGGAG
lmna c. 316_319 del GTGC, p. E108TfsX5

Figure 2

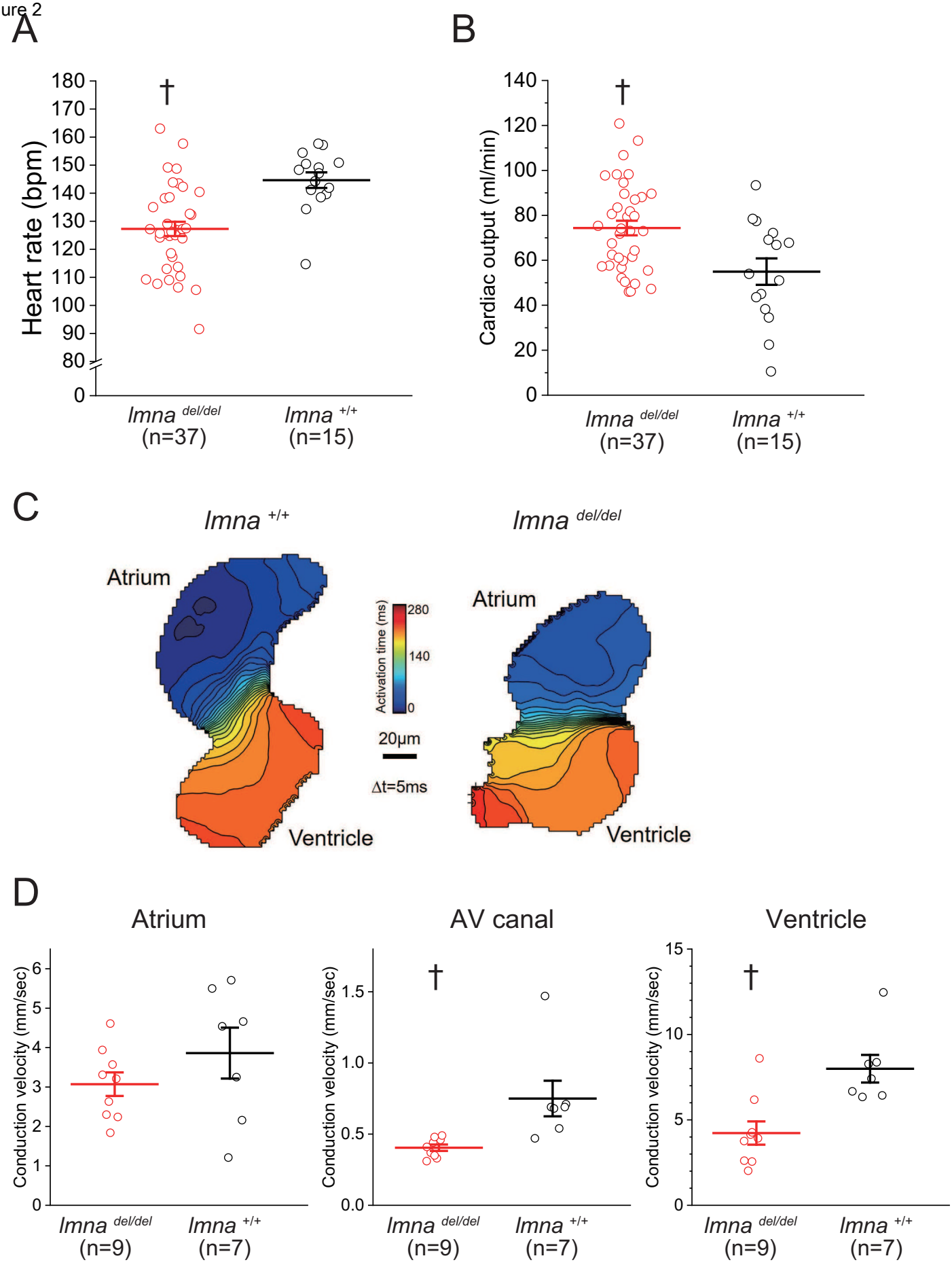
A
Heart rate (bpm)
180
170
160
150
140
130
120
110
100
90
80
0
†
lmna del/del
(n=37)
lmna +/+
(n=15)
B
Cardiac output (ml/min)
140
120
100
80
60
40
20
0
†
lmna del/del
(n=37)
lmna +/+
(n=15)
C
lmna +/+
lmna del/del
Atrium
Ventricle
Activation time (ms)
280
140
0
20μm
Δt=5ms
Atrium
Ventricle
D
Atrium
AV canal
Ventricle
Conduction velocity (mm/sec)
6
5
4
3
2
1
0
1.5
1.0
0.5
0.0
15
10
5
0
†
lmna del/del
(n=9)
lmna +/+
(n=7)

Figure 3

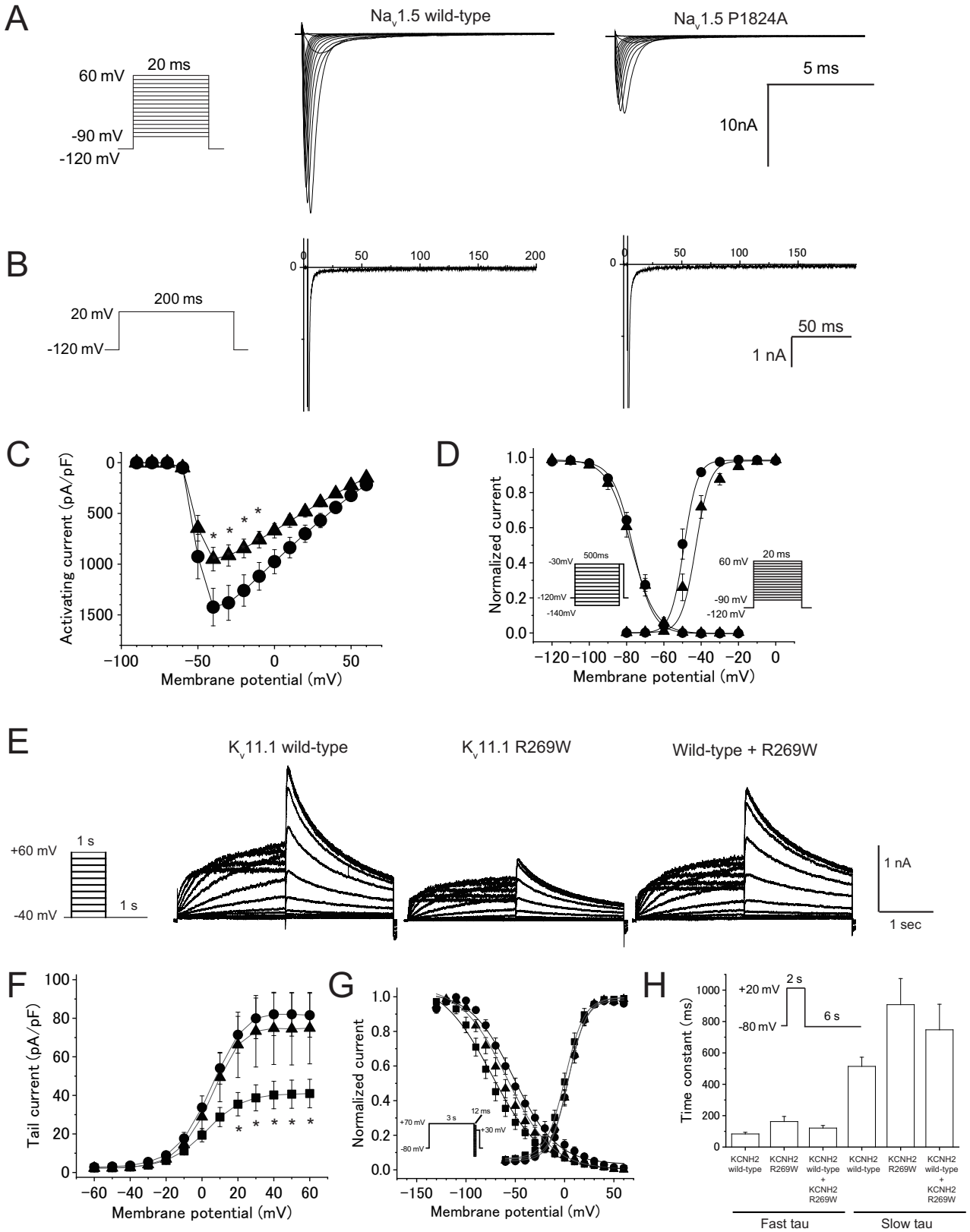
A
Na$_v$1.5 wild-type
Na$_v$1.5 P1824A
20 ms
60 mV
-90 mV
-120 mV
5 ms
10nA
B
200 ms
20 mV
-120 mV
50 ms
1 nA
C
Activating current (pA/pF)
Membrane potential (mV)
D
Normalized current
Membrane potential (mV)
-30mV
500ms
-120mV
-140mV
60 mV
20 ms
-90 mV
-120 mV
E
K$_v$11.1 wild-type
K$_v$11.1 R269W
Wild-type + R269W
+60 mV
1 s
-40 mV
1 nA
1 sec
F
Tail current (pA/pF)
Membrane potential (mV)
G
Normalized current
Membrane potential (mV)
+70 mV
3 s
12 ms
+30 mV
-80 mV
H
Time constant (ms)
+20 mV
2 s
-80 mV
6 s
KCNH2 wild-type
KCNH2 R269W
KCNH2 wild-type + KCNH2 R269W
Fast tau
Slow tau

Figure 4

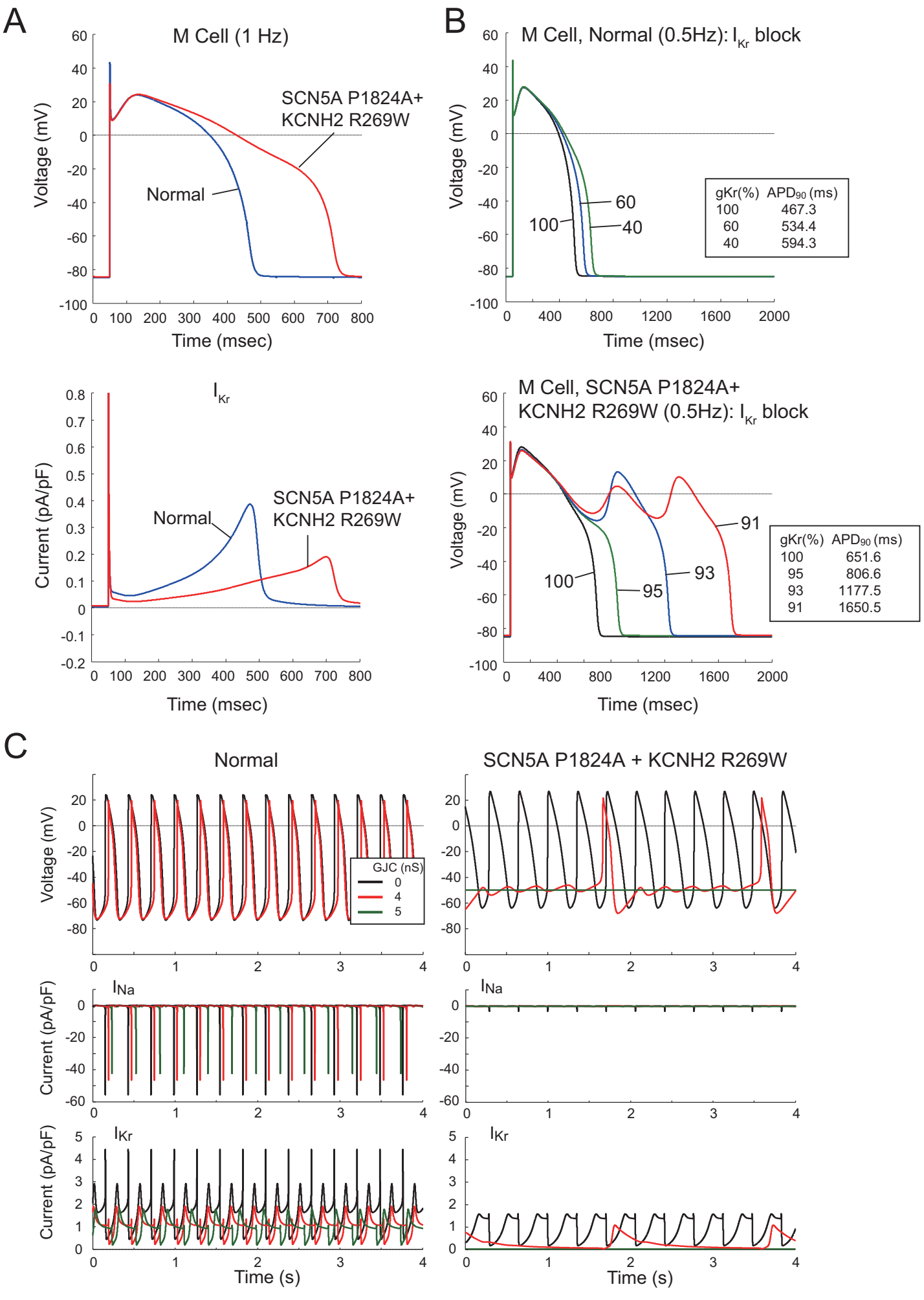
A
M Cell (1 Hz)
SCN5A P1824A+
KCNH2 R269W
Normal
Voltage (mV)
Time (msec)
B
M Cell, Normal (0.5Hz): I_Kr block
60
40
100
gKr(%) APD90 (ms)
100 467.3
60 534.4
40 594.3
I_Kr
Normal
SCN5A P1824A+
KCNH2 R269W
Current (pA/pF)
M Cell, SCN5A P1824A+
KCNH2 R269W (0.5Hz): I_Kr block
91
93
95
100
gKr(%) APD90 (ms)
100 651.6
95 806.6
93 1177.5
91 1650.5
C
Normal
SCN5A P1824A + KCNH2 R269W
GJC (nS)
0
4
5
I_Na
I_Kr
Time (s)

Figure 5

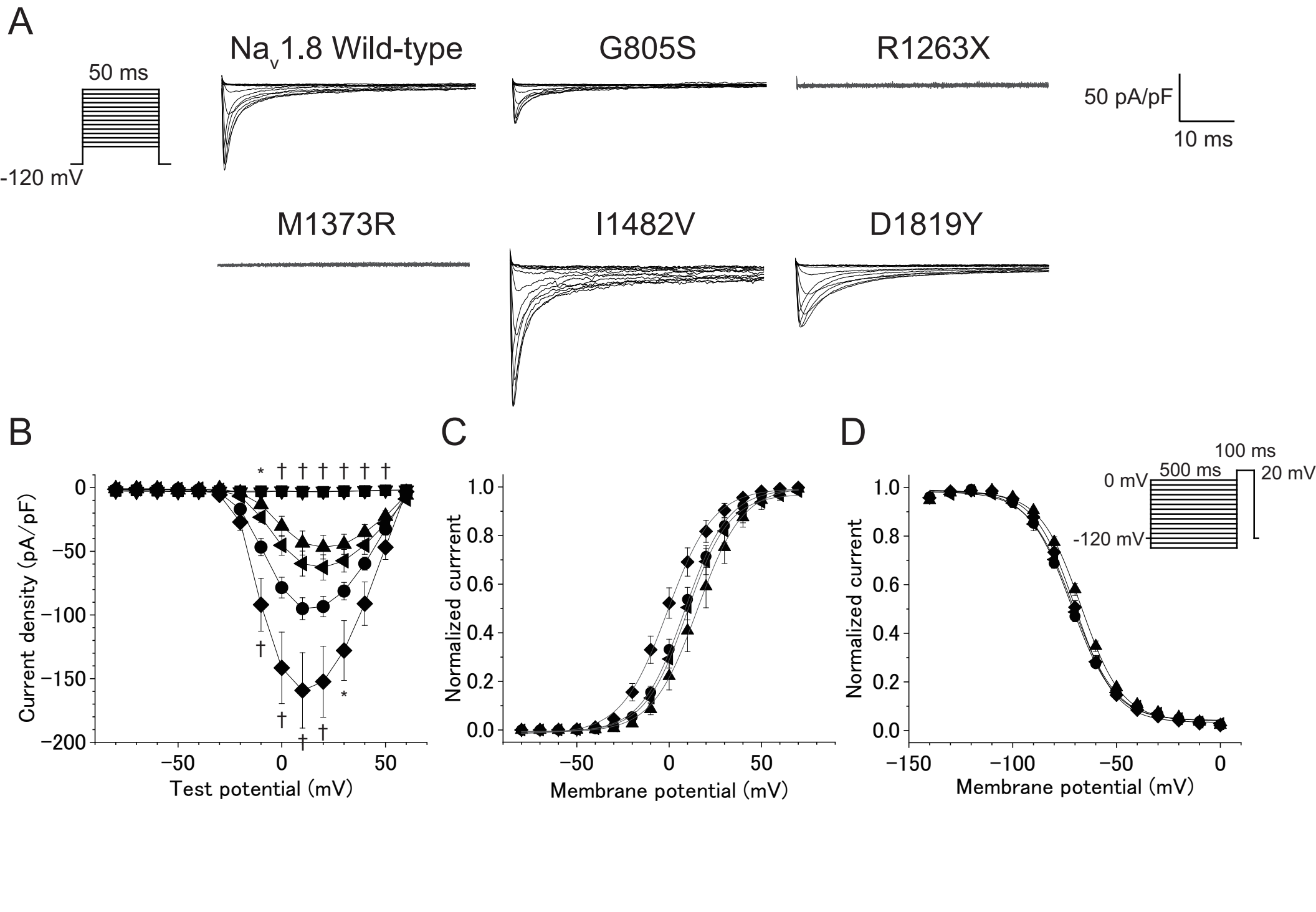
A
50 ms
-120 mV
Na$_v$1.8 Wild-type
G805S
R1263X
50 pA/pF
10 ms
M1373R
I1482V
D1819Y
B
Current density (pA/pF)
Test potential (mV)
C
Normalized currrent
Membrane potential (mV)
D
Normalized current
Membrane potential (mV)
100 ms
500 ms
0 mV
20 mV
-120 mV

SUPPLEMENTARY DATA

Impact of functional studies on interpretation of exome sequence variants in patients with early-onset cardiac conduction-system diseases

Kenshi Hayashi[1], Akihiro Nomura[1], Ryota Teramoto[1,2], Yoshihiro Asano[3], Manu Beerens[2], Yasutaka Kurata[4], Noboru Fujino[1], Hiroshi Furusho[1], Kenji Sakata[1], Eva Buys[2], Patrick Sips[2,5], Micah L. Burch[2], Yanbin Zhao[2], Amy E. Kelly[2], Masanobu Namura[6], Yoshihito Kita[7], Taketsugu Tsuchiya[8], Bunji Kaku[9], Kotaro Oe[10], Yuko Takeda[1], Tetsuo Konno[1], Masaru Inoue[11], Takashi Fujita[12], Takeshi Kato[1], Akira Funada[1], Hayato Tada[1], Akihiko Hodatsu[1], Chiaki Nakanishi[1], Yuichiro Sakamoto[13], Toyonobu Tsuda[1], Yoji Nagata[1], Yoshihiro Tanaka[1], Hirofumi Okada[1], Calum A MacRae[2], Seiji Takashima[14], Masakazu Yamagishi[1, 15], Masa-aki Kawashiri[1], and Masayuki Takamura[1].

Supplementary methods

Study patients

The study conformed with the principles outlined in the Declaration of Helsinki and was approved by the Ethics Committee for Medical Research at our institution. All study patients provided written informed consent before registration.

The study patients were recruited from multiple hospitals in Japan. Early-onset cardiac conduction system disease (CCSD) was defined as bradyarrhythmia occurring in individuals aged <65 years, who showed an atrioventricular (AV) block and/or a sick sinus syndrome (SSS) with pacemaker implantation (PMI) or a family history of PMI. AV block was defined as one of the following conditions: (1) every atrial impulse conducted to the ventricles, regular rate, but the PR interval exceeds 0.20 s (first-degree AV block), (2) blocking of some atrial impulses conducted to the ventricle at a time when physiological interference is not involved (second-degree AV block), or (3) no atrial activity is conducted to the ventricles (third-degree AV block). Sick sinus syndrome was defined as one of the following conditions: (1) persistent spontaneous sinus bradycardia not caused by drugs and inappropriate for the physiological circumstance, (2) sinus arrest or exit block, (3) combinations of sinoatrial (SA) and AV conduction disturbances, or (4) alternation of paroxysms of rapid regular or irregular atrial tachyarrhythmias and periods of slow atrial and ventricular rates. In addition, we used the DNA sequencing data of 102 control subjects without electrocardiogram abnormality.

DNA isolation and whole-exome DNA sequencing

Genomic DNA was extracted from peripheral blood leukocytes by using standard methods[1]. Five micrograms of genomic DNA of the patients was submitted to TAKARA BIO INC. (Kusatsu, Shiga, Japan) for whole-exome sequencing (WES). Exome capture was completed with SureSelect Human All Exon V5 + mtDNA (Agilent, Santa Clara, CA, USA). Exome sequencing was performed using the Illumina HiSeq platform (Illumina, San Diego, CA, USA). We used the Borrows–Wheeler Aligner Maximal Exact Match algorithm to align sequencing reads to human reference genome (build 37). We also used the Genome Analysis Toolkit (GATK ver.3.6) to perform reads' realignments and base quality recalibrations. We set the sensitivity of the Variant Quality Score Recalibration threshold as 99.6% and 95% for single nucleotide variants and insertions/deletions, respectively. After the above standard quality control, we selected only the variants that were absent in the in-house WES data from 102 control individuals without early-onset CCSD. Of those, we extracted the variants in 117 candidate genes linked to arrhythmogenic disorders or cardiomyopathy for further analyses (Supplemental Table 1).

Pathogenicity of candidate variants

We interpreted the sequence variants using 2015 ACMG standards and guidelines, which provided criteria for the classification of pathogenic or likely pathogenic variants.[2] Each pathogenic criterion

is weighted as very strong (PVS1), strong (PS1–4), moderate (PM1–6), or supporting (PP1–5). Rare variants were defined as those with minor allele frequency <0.5% in East Asian at the Human Genetic Variation Database (HGVD) version 2.3 and the Genome Aggregation Database (gnomAD) version 2.0.2. Variants which were absent from these databases were considered as PM2. We selected protein-truncating variants (PTVs) in known genes associated with CCSD (PVS1), or rare missense variants registered as pathogenic or disease-causing mutation associated with CCSD in disease database including ClinVar and Human Gene Mutation Database (HGMD) (PP5). All variants were annotated by the Variant Effect Predictor version 82 and referred following *in silico* damaging scores: MetaSVM for missense variants; LOFTEE for PTVs; and CADD for all variants.[3] MetaSVM score incorporated 10 scores (SIFT, PolyPhen-2 HDIV, PolyPhen-2 HVAR, GERP++, MutationTaster-2, Mutation Assessor, FATHMM, LRT, SiPhy, PhyloP) and the maximum frequency observed in 1000 genome populations. We used the MetaSVM scores from dbNSFP ver.2.9.1. [4] CADD score of 15 indicated that the variant is predicted to be among the 15% most deleterious substitutions that can occur in the human genome. When multiple lines of these in silico prediction algorithms supported a deleterious effect on the gene, the supporting pathogenic evidence of PP3 was assigned. We further sought to determine the relationship between the clinical phenotype (bradyarrhythmia) and the genotype for probands and their relatives in whom a variant was identified (PP1 or PP4). These segregation analyses were performed in the family members as much as possible. If the missense variants are common causes of the disorder and the gene also has very few benign variants, then a missense variant in this gene can be supporting evidence for pathogenicity (PP2). Functional studies were performed using cellular electrophysiological analysis, mathematical modeling, and simulations, and CRISPR/Cas9 mediated gene knock-out in zebrafish to confirm the pathogenicity of detected variants (PS3 or BS3). For a given variant, we selected the criteria based on the evidence observed for the variant. The criteria then are combined according to the scoring rules to choose a classification from the five-tier system[2].

CRISPR-mediated deletions of the human *LMNA* ortholog, *lmna*, in zebrafish

All zebrafish experiments have been approved by Institutional Animal Care and Use Committee (protocol# BWH 2016N000276), which is certified by the Association for Assessment and Accreditation of Laboratory Animal Care. Zebrafish euthanasia was performed following NIH (https://oacu.oir.nih.gov/animal-research-advisory-committee-guidelines) and American Veterinary Medical Association guidelines using an overdose of Tricaine (M-222 or 3-aminobenzoic acid ethyl ester) in combination with hypothermic shock.

The gene editing in zebrafish with CRISPR/Cas9 was conducted to evaluate detected PTV in the *LMNA* gene from patients with early-onset CCSD. The target site of the human *LMNA* ortholog, *lmna*, in zebrafish was selected using a CHOPCHOP webtool, which ranks target sites based on potential off-target effects (5'-GGAGCTCAGCAAAGTGCGTG-3'). Single guide (sg) RNA was generated by in vitro transcription from oligonucleotide-based templates with a MEGAshortscript™ T7 Transcription Kit (Thermo Fisher Scientific Inc., Waltham, MA, USA). DNA double-strand breaks (DSBs) introduced by CRISPR at the target site can be repaired through error-prone nonhomologous end-joining (NHEJ) pathway. The DSB repair by NHEJ could generate indel mutations, which can cause frame shift and then abolish gene function if the mutations occur in an exon. Two microliters of sgRNA stock (400 ng/μl) was mixed with 2 μl of recombinant Cas9 protein (1 μg/μl) (PNA Bio, Newbury Park, CA, USA) and 2μl of water, then incubated on ice for 5 min to allow formation of the sgRNA/Cas9 complex. One nanoliter of the injection mix was injected intracellularly in one-cell stage zebrafish embryos by using glass needles and a micromanipulator. Zebrafish embryos were maintained in E3 water at 28°C.

Cardiac phenotypes were scored at 48 and 72 hpf, and genomic DNA was prepared from 10 individuals for Sanger sequencing. The heart rate was visually counted at 48 hpf by using a stereomicroscope. Cardiac function was evaluated at 48 hpf by using video microscopy with an Axioplan (Zeiss) upright microscope. 816 flames (magnification, 10×; frame rate, 250/s) were

captured, and sequential still frames were analyzed by Image J. Voltage mapping was recorded on isolated 72 hpf zebrafish hearts [5]. Dissected hearts were stained with FluoVolt (Thermo Fisher Scientific Inc., Waltham, MA, USA) and immobilized with blebbistatin or Cytochalasin D (Sigma-Aldrich, St. Louis, MO, USA) for the measurement of action potentials. Fluorescence intensities were recorded with a high-speed charge coupled-device camera (RedShirtImaging, Decatur, GA, USA). Acquired fluorescence images were exported as tiff stacks and analyzed using Matlab software (Mathworks, Natick, MA, USA).

Mosaic founders (F0) were raised and outcrossed to a wild-type line at the age of 3 months. Sequencing analysis of F1 fish after outcross was performed at the age of 5 months, and various truncating indels of *lmna* gene were confirmed. Heterozygous F1 fishes with same *lmna* mutation were incrossed, and cardiac phenotypes for F2 embryos were evaluated as stated above. Each F2 embryo was genotyped after evaluation of the cardiac phenotype to distinguish between heterozygous and homozygous carriers.

Plasmid constructs and transfection of mammalian cell lines

The *KCNH2* cDNA in the mammalian expression vector pSI, the *SCN5A* cDNA in the pCGI vector [6], *SCN1B* cDNA in the IRGFP vector, and the *SCN10A* cDNA in the pIRES2-EGFP plasmid were kindly provided by Dr. Sabina Kupershmidt and Dr. Dan Roden (Vanderbilt University). Mutant cDNAs were constructed by an overlap extension strategy or using a QuikChange XL Site-Directed Mutagenesis Kit (Agilent Technologies, Santa Clara, CA, USA). With regard to the study of Nav1.5 current, HEK293 cells were transiently transfected with wild-type *SCN5A* cDNA (0.5 μg), or mutant *SCN5A* cDNA (0.5 μg), using a FuGENE 6 Transfection Reagent (Roche Applied Science, Penzberg, Germany). Cells were cotransfected with the same amount of *SCN1B* cDNA in the IRGFP vector as each sodium channel cDNA. With regard to the studies of Kv11.1 current, CHO-K1 cells were transiently transfected with wild-type *KCNH2* cDNA (0.5 μg) or mutant *KCNH2* cDNA (0.5 μg), using a FuGENE 6 Transfection Reagent (Roche Applied Science, Penzberg, Germany). Cells were cotransfected with the same amount of green fluorescent protein (GFP) as each potassium channel cDNA. With regard to the study of Nav1.8 current, ND 7/23 cells were transiently transfected with 3 μg of the cDNA encoding human wild-type or variant Nav1.8, using an X-tremeGENE 9 DNA Transfection Reagent (Roche Applied Science, Penzberg, Germany). ND 7/23 cells were kindly provided by Dr. Naomasa Makita (Nagasaki University). Cells displaying green fluorescence 48–72 h after transfection were subjected to electrophysiological analysis.

Electrophysiology and data analysis

Potassium or sodium currents were studied using the whole-cell patch clamp technique with an amplifier, Axopatch-200B (Molecular Devices, Sunnyvale, CA), at room temperature (23°C-25°C for potassium currents and 20°C–22°C for sodium currents). Electrode resistance ranged from 2 to 4 MΩ and from 0.8 to 1.5 MΩ for potassium and sodium channel recordings, respectively. The voltage clamp protocols are described in the Figures. Data were acquired using pCLAMP software (v. 9; Molecular Devices, Sunnyvale, CA, USA). Data acquisition and analysis were performed using a Digidata 1321 A/D converter and pCLAMP8.2 software (Molecular Devices, Sunnyvale, CA, USA). While recording potassium currents, the pipette solution (intracellular solution) contained 110 mM KCl, 5 mM K_2ATP, 2 mM $MgCl_2$, 10 mM HEPES, and 5 mM K_4BAPTA at pH 7.2, and the bath solution contained 140 mM NaCl, 5.4 mM KCl, 2 mM $CaCl_2$, 1.0 mM $MgCl_2$, 10 mM HEPES, and 10 mM glucose, adjusted to pH 7.4 with NaOH. While recording Nav1.5 currents, the pipette solution (intracellular solution) contained 10 mM NaF, 110 mM CsF, 20 mM CsCl, 10 mM EGTA, and 10 mM HEPES at pH 7.35 with CsOH. The bath solution contained 145 mM NaCl, 1.5 mM $CaCl_2$, 4.5 mM KCl, 1 mM $MgCl_2$, 10 mM HEPES, and 5 mM glucose, adjusted to pH 7.4 with CsOH. While recording Nav1.8 currents, the pipette solution (intracellular solution) contained 10 mM NaF, 110 mM CsF, 20 mM CsCl, 5 mM EGTA, 10 mM HEPES, and 5 mM Mg2-ATP, with a pH of 7.3 adjusted with

CsOH. The bath solution contained 135 mM NaCl, 1.8 mM CaCl2, 1.0 mM MgCl2, 20 mM TEA-Cl, 10 mM HEPES, and 10 mM glucose, with a pH of 7.4, adjusted with NaOH. Endogenous tetrodotoxin (TTX)-sensitive I_{Na} and L- and T-type calcium currents were eliminated with TTX 200 nM, nisoldipine 1 μM and NiCl2 200 μM, respectively.

The voltage dependence of potassium current activation was determined for each cell by fitting peak values of tail current (I_{tail}) versus test potential to a Boltzmann function in the following form: $I_{tail}=I_{tail\text{-}max}/\ \{1+\exp[(V_{1/2}-V_t)/k]\}$, where $I_{tail\text{-}max}$ is peak I_{tail}, V_t is the test potential, $V_{1/2}$ is the voltage at which I_{tail} is half of $I_{tail\text{-}max}$, and k is the slope factor [7]. Steady-state inactivation of the potassium current was analyzed as previously described[8]. Briefly, the corrected steady-state inactivation curves were fitted with a Boltzmann function in the following form: $I/(I_{ma}-I_{min}) = 1/\ \{1+\exp[(V_t-V_{1/2})/k]\}\ + I_{min}$, where I is the amplitude of the inactivating current corrected for deactivation, I_{max} is the maximum of I, I_{min} is the minimum of I, V_t is the prepulse of test potential, $V_{1/2}$ is the voltage at which I is half of I_{max}, and k is the slope factor. Deactivation rates of Kv11.1 channels were measured using a two-step voltage protocol and by fitting tail currents with two exponential functions [7].

The parameters for voltage dependence of sodium current activation were estimated from the current–voltage relationship based on the Boltzmann equation in the following form: $I = G_{max} \times (V - V_{rev}) \times (1 + \exp[V - V_{1/2}]/k)^{-1}$, where I is the peak Na current during the test pulse potential V. The parameters estimated by the fitting are G_{max} (maximum conductance), V_{rev} (reversal potential), and k (slope factor) [9]. Steady-state availability for fast inactivation was measured with a standard double-pulse protocol, and the data were fit with the Boltzmann equation in the following form: $I/I_{max} = (1 + \exp[(V - V_{1/2})/k])^{-1}$, where I_{max} is the maximum peak Na current, to determine the membrane potential for $V_{1/2}$ and k [9].

Mathematical modeling and simulations

With mathematical models of human ventricular myocytes [10] and rabbit peripheral sinoatrial node (SAN) cells [11], the effects of the changes in kinetic behavior of I_{Kr} and I_{Na} on the mid-myocardial action potential configuration of the ventricular myocyte model and pacemaker activity of the peripheral SAN cell model connected to the atrial membrane model via the gap junction conductance were evaluated. Dynamic behaviors of the model cell were determined by solving a system of nonlinear ordinary differential equations numerically. Numerical integration was performed on Workstation HP xw9400 with MATLAB 7.5 (The MathWorks, Inc., Natick, MA, USA). The numerical algorithms available as a MATLAB ODE solver, *ode15s* (a variable time-step numerical differentiation approach selected for its suitability to stiff systems) were used.

Statistical analysis

Pooled electrophysiological data were expressed as mean±standard error. Two-tailed Student's *t*-test was used for single comparisons between two groups. One-way ANOVA, followed by a Bonferroni *post hoc* test, was used to analyze data with equal variance among three or more groups. A value of $P<0.05$ was considered statistically significant. Statistical analysis was performed using JMP Pro 11.0.0 (SAS Institute Inc., NC, USA) and Origin 2018 (OriginLab, Northampton, MA, USA).

Supplemental Figure Legends

Supplemental Figure 1. Generation of patient-specific mutant lines in zebrafish using CRISPR-mediated deletions of the human *LMNA* ortholog, *lmna*, in zebrafish.

Supplemental Figure 2. Functional studies of PTV, *LMNA* c.339dupT using CRISPR-mediated deletions of the human *LMNA* ortholog, *lmna*, in zebrafish .
(A) CRISPR/ Cas9-edited embryo at 48 hpf and Sanger sequence of *lmna* gene. (B) Heart rate of CRISPR/Cas9-injected embryos (n=66), CRISPR-only injected embryos (n=37), and non-injected embryos (n=61). †P<0.01 vs. Crispr only or non-injected by one-way ANOVA, followed by a Bonferroni *post hoc* test. (C) Isochronal map of CRISPR/ Cas9 - edited embryo and CRISPR only injected embryos summarizing the regional spread of electrical activity across the atrium and into the ventricle. The lines represent the positions of the action potential wavefront at 5-ms intervals. Mean estimated conduction velocities of ventricle from CRISPR/ Cas9 - edited embryo with indels of *lmna* gene. †P<0.01 vs. CRISPR only by two-tailed Student's t-test. PAM, protospacer adjacent motif

Supplemental References

1. Nomura A, Tada H, Teramoto R, Konno T, Hodatsu A, Won HH, Kathiresan S, Ino H, Fujino N, Yamagishi M, Hayashi K. Whole exome sequencing combined with integrated variant annotation prediction identifies a causative myosin essential light chain variant in hypertrophic cardiomyopathy. *J Cardiol*. 2016;67:133-139.
2. Richards S, Aziz N, Bale S, Bick D, Das S, Gastier-Foster J, Grody WW, Hegde M, Lyon E, Spector E, Voelkerding K, Rehm HL, Committee ALQA. Standards and guidelines for the interpretation of sequence variants: a joint consensus recommendation of the American College of Medical Genetics and Genomics and the Association for Molecular Pathology. *Genet Med*. 2015;17:405-424.
3. McLaren W, Pritchard B, Rios D, Chen Y, Flicek P, Cunningham F. Deriving the consequences of genomic variants with the Ensembl API and SNP Effect Predictor. *Bioinformatics*. 2010;26:2069-2070.
4. Liu X, Jian X, Boerwinkle E. dbNSFP v2.0: a database of human non-synonymous SNVs and their functional predictions and annotations. *Hum Mutat*. 2013;34:E2393-2402.
5. Panakova D, Werdich AA, Macrae CA. Wnt11 patterns a myocardial electrical gradient through regulation of the L-type Ca(2+) channel. *Nature*. 2010;466:874-878.
6. Fukuda K, Davies SS, Nakajima T, Ong BH, Kupershmidt S, Fessel J, Amarnath V, Anderson ME, Boyden PA, Viswanathan PC, Roberts LJ, 2nd, Balser JR. Oxidative mediated lipid peroxidation recapitulates proarrhythmic effects on cardiac sodium channels. *Circ Res*. 2005;97:1262-1269.
7. Hayashi K, Shimizu M, Ino H, Yamaguchi M, Mabuchi H, Hoshi N, Higashida H. Characterization of a novel missense mutation E637K in the pore-S6 loop of HERG in a patient with long QT syndrome. *Cardiovasc Res*. 2002;54:67-76.
8. Smith PL, Baukrowitz T, Yellen G. The inward rectification mechanism of the HERG cardiac potassium channel. *Nature*. 1996;379:833-836.
9. Makita N, Behr E, Shimizu W, et al. The E1784K mutation in SCN5A is associated with mixed clinical phenotype of type 3 long QT syndrome. *J Clin Invest*. 2008;118:2219-2229.
10. Kurata Y, Hisatome I, Matsuda H, Shibamoto T. Dynamical mechanisms of pacemaker generation in IK1-downregulated human ventricular myocytes: insights from bifurcation analyses of a mathematical model. *Biophys J*. 2005;89:2865-2887.
11. Kurata Y, Matsuda H, Hisatome I, Shibamoto T. Regional difference in dynamical property of sinoatrial node pacemaking: role of na+ channel current. *Biophys J*. 2008;95:951-977.

Supplemental Table 1 CCSD candidate 117 genes linked to arrhythmogenic diseases or cardiomyopathies

ABCC9	*COL3A1*	*ILK*	*MAP2K1*	*PRKAG2*	*TBX5*
ACTA2	*CRYAB*	*JPH2*	*MAP2K2*	*PTPN11*	*TCAP*
ACTC1	*CSRP3*	*JUP*	*MOG1*	*RAF1*	*TGFB3*
ACTN2	*DES*	*KCNA5*	*MYBPC3*	*RBM20*	*TGFBR1*
AKAP9	*DMD*	*KCND3*	*MYH6*	*RYR2*	*TGFBR2*
ANKB	*DMPK*	*KCNE1*	*MYH7*	*SCN10A*	*TMEM43*
ANKRD1	*DSC2*	*KCNE2*	*MYH11*	*SCN1B*	*TMPO*
BAG3	*DSG2*	*KCNE3*	*MYL2*	*SCN2B*	*TNNC1*
BRAF	*DSP*	*KCNE5*	*MYL3*	*SCN3B*	*TNNI3*
CACNA1C	*EMD*	*KCNH2*	*MYLK*	*SCN4B*	*TNNT2*
CACNA2D1	*EYA4*	*KCNJ2*	*MYLK2*	*SCN5A*	*TPM1*
CALM1	*FBN1*	*KCNJ3*	*MYO6*	*SGCD*	*TRDN*
CALM2	*FBN2*	*KCNJ5*	*MYOZ2*	*SHOC2*	*TRPM4*
CALM3	*FXN*	*KCNJ8*	*MYPN*	*SLAMP*	*TTN*
CALR3	*GJA1*	*KCNN2*	*NEXN*	*SLC2A10*	*TTR*
CASQ2	*GJA5*	*KCNQ1*	*NKX2.5*	*SLC8A1*	*TXNRD2*
CAV3	*GLA*	*KRAS*	*NRAS*	*SMAD3*	*VCL*
CBL	*GPD1L*	*LAMP2*	*PDLIM3*	*SNTA1*	
CBS	*HCN4*	*LDB3*	*PKP2*	*SOS1*	
CMK2D	*HRAS*	*LMNA*	*PLN*	*TAZ*	

Supplemental Table 2 Overview of detected rare variants of patients with early-onset CCSD

Gene	Base change	Amino acid change	gnomAD (East Asian)	HGVD (JPN)	MetaSVM	CADD Score	LOFTEE	Novelty (ClinVar)	Novelty (HGMD)
EMD	677 G>A	W226X	NA	NA	NA	39	HC	Not registered	DM for EDMD
	664C>T	Q222X	NA	NA	NA	37	HC	Not registered	Not registered
LMNA	339dupT	K114XfsX1	NA	NA	NA	34	HC	Likely pathogenic	Not registered
	1489-2A>G		NA	NA	NA	24.9	HC	Not registered	DM for cardiac disease
	961C>T	R321X	NA	NA	NA	37	HC	Pathogenic	DM for DCM
KCNA5	1580C>T	T527M	0.0016	0.0017	D	25.2	NA	Uncertain significance	DM for AF+SSS
KCNH2	805C>T	R269W	NA	NA	D	27.2	NA	Not provided	DM for LQTS+SSS
SCN5A	5470C>G	P1824A	NA	NA	D	24.6	NA	Not provided	DM for LQTS+SSS
HCN4	2845C>T	R949W	0.0010	0.0016	D	23.2	NA	Not registered	Not registered
SCN10A	3787C>T	R1263X	NA	NA	NA	48	HC	Not registered	Not registered
	4444A>G	I1482V	NA	NA	D	19.0	NA	Not registered	Not registered
	5455G>T	D1819Y	NA	NA	D	31	NA	Not registered	Not registered
	4118T>G	M1373R	NA	NA	D	28.2	NA	Uncertain significance	Not registered
	1519T>C	F507L	NA	NA	D	22.4	NA	Not registered	Not registered
	2413G>A	G805S	NA	NA	D	32	NA	Not registered	Not registered
RYR2	2300C>G	S767W	NA	0.0004	D	34	NA	Not registered	Not registered
MYH6	3347G>A	R1116H	0.000065	0.0004	D	28	NA	Uncertain significance	Not registered
	3755G>A	R1252Q	NA	NA	D	27.3	NA	Not registered	Not registered
MYH7	968T>C	I323T	NA	NA	D	24.1	NA	Uncertain significance	VUS for HCM
MYH11	4532G>A	R1511Q	NA	NA	D	34	NA	Not registered	Not registered
RBM20	3545G>A	R1182H	0.0022	0.0008	D	34	NA	Conflicting interpretations of pathogenicity	DM for DCM
	3649G>A	G1217R	NA	0.0008	D	28.3	NA	Uncertain significance	Not registered
TTN	70264G>C	G23422R	0.00012	0.0004	D	22.3	NA	Not registered	Not registered
DES	556G>A	D186N	NA	NA	D	24.7	NA	Not registered	Not registered
CBS	1552T>C	Y518H	NA	NA	D	17.9	NA	Not registered	Not registered
TBX5	409G>A	V137M	NA	0.0004	D	32	NA	Not registered	Not registered

ACTC1	710C>T	S237F	NA	NA	D	29.2	NA	Not registered	Not registered
PRKAG2	1366C>G	R456G	0.000058	NA	D	23.7	NA	Not registered	Not registered
MAP2K2	937C>T	R313W	NA	NA	D	27.1	NA	Uncertain significance	Not registered

gnomAD, Genome Aggregation Database; HGVD, Human Genetic Variation Database; MetaSVM, in silico ensemble damaging score; CADD, combined annotation dependent depletion; LOFTEE, loss-of-function transcript effect estimator; HGMD, human gene mutation database; NA, not available; D, rare damaging variants; HC, high-confidence; DM, disease causing mutation; EDMD, Emery-Dreifuss muscular dystrophy; DCM, dilated cardiomyopathy, AF, atrial fibrillation; LQTS, long QT syndrome, HCM, hypertrophic cardiomyopathy; VUS, variant of unknown significance.